Monthly Notices
of the
ROYAL ASTRONOMICAL SOCIETY

Mon. Not. R. Astron. Soc. **406,** 1435–1459 (2010) doi:10.1111/j.1365-2966.2010.16780.x

The nature of proximate damped Lyman α systems★

Sara L. Ellison,[1]† J. Xavier Prochaska,[2] Joseph Hennawi,[3] Sebastian Lopez,[4] Christopher Usher,[1] Arthur M. Wolfe,[5] David M. Russell[6] and Chris R. Benn[7]

[1]*Department of Physics and Astronomy, University of Victoria, Victoria, British Columbia, V8P 1A1, Canada*
[2]*Department of Astronomy and Astrophysics, UCO/Lick Observatory, University of California, 1156 High Street, Santa Cruz, CA 95064, USA*
[3]*Department of Astronomy, 601 Campbell Hall, University of California, Berkeley, CA 94720-3411, USA*
[4]*Departamento de Astronomía, Universidad de Chile, Casilla 36-D, Santiago, Chile*
[5]*Department of Physics, Center for Astrophysics and Space Sciences, University of California, San Diego, 9500 Gilman Drive, La Jolla, CA 92093-0424, USA*
[6]*Astronomical Institute 'Anton Pannekoek', University of Amsterdam, PO Box 94249, 1090 GE Amsterdam, Netherlands*
[7]*Isaac Newton Group, Apartado 321, E-38700 Santa Cruz de La Palma, Spain*

Accepted 2010 April 2. Received 2010 March 30; in original form 2009 December 21

ABSTRACT

We present high-resolution echelle spectra of seven proximate damped Lyman α (PDLA) systems. The relative velocity separation of each PDLA from the background quasar is $\Delta V < 3000$ km s^{-1}. Combining our sample with a further nine PDLAs from the literature we compare the chemical properties of the proximate systems with a control sample of intervening DLAs. The PDLAs are usually excluded from statistical studies of absorption-selected galaxies and this sample constitutes the first systematic study of their chemical and ionization properties. Taken at face value, the sample of 16 PDLAs exhibits a wide range of metallicities, ranging from $Z \sim 1/3$ to $\sim 1/1000\,Z_{\odot}$, including the DLA with the lowest N(Si II)/N(H I) yet reported in the literature. However, some of these abundances may require ionization corrections. We find several pieces of evidence that indicate enhanced ionization and the presence of a hard ionizing spectrum in PDLAs which lead to properties that contrast with the intervening DLAs, particularly when the N(H I) is low. The abundances of Zn, Si and S in PDLAs with log N(H I) > 21, where ionization corrections are minimized, are systematically higher than the intervening population by a factor of around 3. We also find possible evidence for a higher fraction of N V absorbers amongst the PDLAs, although the statistics are still modest. 6/7 of our echelle sample show high ionization species (Si IV, C IV, O VI or N V) offset by >100 km s^{-1} from the main low ion absorption. We analyse fine-structure transitions of C II★ and Si II★ to constrain the PDLA distance from the quasi-stellar object (QSO). Lower limits range from tens of kpc to >160 kpc for the most stringent limit. We conclude that (at least some) PDLAs do exhibit different characteristics relative to the intervening population out to 3000 km s^{-1} (and possibly beyond). None the less, the PDLAs appear distinct from lower column density associated systems, and the inferred QSO–absorber separations mean they are unlikely to be associated with the QSO host. No trends with ΔV are found, although this requires a larger sample with better emission redshifts to confirm. We speculate that the PDLAs preferentially sample more massive galaxies in more highly clustered regions of the high-redshift Universe.

Key words: galaxies: abundances – galaxies: high redshift – galaxies: ISM – quasers: absorption lines.

1 INTRODUCTION

Absorption systems with 13 < log$N$(H I) < 17 and within ∼5000 km s^{-1} of a background quasi-stellar object (QSO) are often considered to be 'associated' with the quasar host galaxy, its immediate environment or its ejecta. Evidence for this conclusion comes from time variability of the absorption (Hamann, Barlow & Junkkarinen 1997a; Wise et al. 2004; Lundgren et al. 2007),

★Based on observations made with ESO Telescopes at the Paranal Observatories under program 080.A-0014(A).
†E-mail: sarae@uvic.ca

partial coverage of the emission source (Hamann et al. 1997b,c; Fox, Bergeron & Petitjean 2008), elevated incidence of highly ionized species (e.g. Ganguly et al. 2001; Richards 2001; Fechner & Richter 2009), possible dependence of absorber incidence on QSO properties such as radio loudness or orientation (Møller & Jakobsen 1987; Richards et al. 2001; Baker et al. 2002; Vestergaard 2003; Wild et al. 2008) and solar or super-solar metallicities (e.g. Petitjean, Rauch & Carswell 1994; Hamann, Barlow & Junkkarinen 1997a; Srianand & Petitjean 2000; D'Odorico et al. 2004; Fechner & Richter 2009). The associated population of absorbers appears to extend out to at least 10 000 km s^{-1} (Petitjean et al. 1994; Richards et al. 1999; Wild et al. 2008; Tytler et al. 2009).

Although the $z_{\rm abs} \sim z_{\rm em}$ Lyα forest, C IV, Mg II and Lyman limit systems have been well-researched in the last 20 years, the same is not true of the proximate damped Lyman α systems (PDLAs). This is partly a historical bias. DLAs are excellent tools for characterizing the high-redshift galaxy population. Knowing that associated systems may be connected with the QSO or its host galaxy, statistical samples of DLAs have therefore excluded these potentially special systems (e.g. Wolfe et al. 1995; Ellison et al. 2001b; Prochaska et al. 2005; Jorgenson et al. 2006; Noterdaeme et al. 2009). Furthermore, the chemical abundances of intervening DLAs can be determined fairly easily because their gas is predominantly neutral. Proximity to a QSO could invalidate that assumption and lead to erroneous abundance determinations, unless photoionization modelling is used. However, it is for exactly these reasons that the study of PDLAs is interesting. PDLAs provide a potential probe of galaxies clustered around (or associated with) QSOs, and even provide insight into the interplay between ionizing radiation and the interstellar medium (ISM).

One of the difficulties in studying the PDLAs is the small redshift path for each line of sight, which means that PDLAs are very rare. For example, assuming the same number density as intervening systems at $z = 3$, ∼100 QSOs would need to be surveyed to find just one PDLA. A second challenge is constructing a sample of PDLAs selected with a homogeneous QSO–absorber velocity offset (ΔV) criterion. Since the derived emission redshift of a QSO depends critically on the emission lines used (e.g. Gaskell 1982; Tytler & Fan 1992), the value can be uncertain by over 1000 km s^{-1} (∼3 Mpc proper at $z = 3$). The first systematic study of PDLAs was conducted with the Complete Optical and Radio Absorption Line System (CORALS) Survey data by Ellison et al. (2002) who found a factor of 4 excess in the number density of PDLAs in their radio-selected sample. Russell, Ellison & Benn (2006) extended this work to identify 33 PDLAs in the Sloan Digital Sky Survey (SDSS) Data Release 3 (DR3) and confirmed the PDLA excess, independent of radio loudness, at 3.5σ significance. In the largest PDLA survey conducted so far, Prochaska et al. (2008b) use the SDSS DR5 to identify 108 PDLAs with $\Delta V < 3000$ km s^{-1}. In addition to its larger size, this work re-calculated the QSO redshifts in order to obtain improved estimates of ΔV. Prochaska et al. (2008b) found that PDLAs outnumber the intervening DLAs at $z \sim 3$ by a factor of 2, but found no statistically significant excess at $z < 2.5$ or > 3.5.

In addition to the PDLA number density, Prochaska et al. (2008b) investigated whether their H I column density distribution function differed from the intervening DLAs. They found marginal evidence for an excess of high N(H I) PDLAs. Previously, Tytler (1982) had found no excess for the slightly lower N(H I) Lyman limit systems. However, with a much larger sample, Prochaska, O'Meara & Worseck (2010) find a deficit. Apart from their incidence and N(H I) distribution, few studies of PDLAs exist to assess whether or not they are consistent with the intervening population. In particular, PDLAs are rarely targeted for echelle spectroscopy, so little is known about their chemical enrichment. None the less, a small number of PDLAs have appeared in chemical abundance studies (see Table 7 for those that meet our criteria) and they do not appear to have strikingly different properties to the intervening DLAs (Lu et al. 1996; Akerman et al. 2005; Rix et al. 2007). The range of metallicities, α element enhancements and dust depletions are all consistent with the range seen amongst intervening DLAs. Rix et al. (2007) also found negligible ionization corrections were necessary for the PDLA in their study, as is usually the case for other DLAs. It has therefore usually been concluded that the PDLAs do not constitute a distinct population from the intervening systems (e.g. Møller, Warren & Fynbo 1998).

In this work, we present echelle spectra for seven PDLAs (Section 2), determine improved emission redshifts (Section 3) and measure column densities for a range of metal line species (Section 4). We supplement our sample with other PDLAs critically selected from the literature to form a sample of 16 proximate absorbers (Section 5). Ionization properties and metal abundances of PDLAs are compared to the intervening systems in Sections 6 and 7. Finally, we use measurements of C II* and upper limits to Si II* to constrain the distance between the PDLA and the background QSO (Section 8).

Unless otherwise stated, we assume $\Omega_{\rm M} = 0.3$, $\Omega_\Lambda = 0.7$ and $H_0 = 70$ km s^{-1} Mpc^{-1}.

2 SAMPLE, OBSERVATIONS AND DATA REDUCTION

PDLAs for this study were mostly selected from the SDSS DR5 catalogue of Prochaska et al. (2008b). These are J014049.18−083942.5, J014214.74+002324.3, J113130+604420, J124020.9+145535.6, J160413.9+395121.9 and J232115.48+142131.5. For simplicity we hereafter refer to these QSOs by their SDSS names in the form Jhhmm+ddmm. One additional non-SDSS QSO is also in the sample: Q0151+048 (UM144). SDSS magnitudes are given in Table 1 for all QSOs except Q0151+048 where we have taken the R-band magnitude from the APM[1] plate measurements. Our target selection was based on relatively bright QSOs with absorbers whose velocity offset was found to be $\Delta V < 3000$ km s^{-1} by Prochaska et al. (2008b), and with positions accessible during our scheduled observing runs. The ΔV cut-off is somewhat arbitrary and it should be stressed that it is unlikely that these velocities correspond to distances inferred from the Hubble expansion [$d = v/H(z)$] if the proximate absorbers are either linked to the host galaxy or associated with its gravitational potential. In the former case, the velocities may reflect outflows or internal motions. In the latter scenario, the ΔV distribution would be indicative of peculiar motions. We provide empirical evidence that the value of ΔV does not correspond to a Hubble distance by showing that a number of the PDLAs have negative velocities relative to the QSO (Section 3) and that elemental trends do not correlate with ΔV (Section 6).

Observations were obtained with either the UV-Visual Echelle Spectrograph (UVES) at the Very Large Telescope (VLT) or the High Resolution Echelle Spectrograph (HIRES) on the Keck telescope.

[1] http://www.ast.cam.ac.uk/∼apmcat

Table 1. Target list and observing journal. The instrument set-up for HIRES refers to the echelle/cross-disperser angles. The S/N is given as a representative value of the final combined spectra of both settings.

QSO	r mag (SDSS)	z_{em}	z_{abs}	log N(H I) (cm^{-2}) (UVES/SDSS)	Instrument	Instrument set-up	Exposure time (s)	S/N pixel^{-1}
J0140−0839	17.7	3.7156	3.6960	20.75 ± 0.15	UVES	346+580	6000	30–50
						437+860	6000	
J0142+0023	18.3	3.3734	3.34765	20.38 ± 0.05	UVES	346+580	6000	30–50
						437+860	10 200	
Q0151+048	17.5	1.9225	1.9342	20.34 ± 0.02	HIRES	0/1.250	9000	15–20
J1131+6044	17.7	2.9069	2.8754	20.50 ± 0.15	HIRES	0/1.680	7200	15–20
J1240+1455	18.9	3.1092	3.1078	21.3 ± 0.2	HIRES	−0.110/0.557	5400	5–8
J1604+3951	18.1	3.1542	3.1633	21.75 ± 0.2	HIRES	−0.110/0.557	10 300	10–15
J2321+1421	18.3	2.5539	2.5731	20.70 ± 0.05	UVES	346+580	3000	10–30
						437+860	11700	

2.1 UVES data acquisition and reduction

UVES is a dual-arm echelle spectrograph with a grating cross-disperser. There are four different cross-dispersers available and two dichroics (DIC1 and DIC2), which split the incident beam between the blue and red arms. The central wavelengths are governed by the grating angles and are adjusted to allow the desired spectral coverage to fall on the three CCDs (one in the blue arm and two in the red). We combined two of UVES's 'standard' settings (DIC1 346+580 and DIC2 437+860) in order to obtain spectral coverage over approximately 3050–9700 Å. Integration times are given in Table 1. Observations of a ThAr lamp for wavelength calibration followed each exposure. The CCDs were binned 2 × 2 and a 1 arcsec slit was used, resulting in nominal resolutions of R = 41 000 and 39 000 in the blue and red arms, respectively. We observed J0140−0839, J0142+0023 and J2321+1421 on the nights of 2007 October 2–3 with UVES in visitor mode. The seeing ranged between 0.6 and 1.0 arcsec.

The spectra were extracted and reduced using the UVES pipeline. The extracted spectra from each exposure were converted to a common vacuum-heliocentric wavelength scale. Where multiple exposures in a given setting were obtained, or where there is spectral overlap between settings, the data were combined, weighting by the inverse of the flux variances. Table 1 lists the typical signal-to-noise ratio (S/N) for each target in the final combined spectrum (where there is some wavelength overlap between settings). The spectrum was normalized by fitting a smooth continuum through unabsorbed parts of the data using the Starlink DIPSO package.[2]

2.2 HIRES data acquisition and reduction

J1240+1455 and J1604+3951 were observed with the Keck/HIRES spectrometer (Vogt 1994) using the upgraded CCD mosaic on 2007 April 27–28. J1131+6044 and Q0151+048 were also observed with HIRES on 2006 December 25 and 2006 August 17, respectively. The first two quasars, which have PDLAs at $z_{abs} < 3$, were observed using the blue cross-disperser (HIRESb) with wavelength coverage from roughly the atmospheric cut-off to ≈6000 Å. The latter two were observed using the red cross-disperser (HIRESr) with the kv418 blocking filter giving an effective wavelength coverage of 4300–8700 Å. The echelle and cross-disperser angles are given in Table 1, along with total exposure times. All of the observations were acquired through the C1 decker which affords a full width at half maximum (FWHM) ≈6 km s^{-1} spectral resolution. The data were reduced with the HIRedux pipeline that is available within the XIDL software package.[3] One significant difference in the analysis of the HIRES data, compared to the UVES reductions, is the stage at which the continuum is fitted. Whereas the UVES data are normalized as the final reduction step once the echelle orders have been combined into one dimension, the XIDL reduction pipeline fits a local continuum to each order before the 2D spectra are combined into 1D. The advantage of this latter approach is that the construction of the 1D spectrum is simplified, e.g. by removing the effects of the blaze. The disadvantage is that since damped Lyα troughs extend over multiple orders, HIRES spectra do not lend themselves easily to Lyα fitting. We discuss this further below.

3 REDSHIFTS

Accurate emission and absorption redshifts are required in order to define a sample of PDLAs lying within a given velocity range ΔV of the QSO. Typical limiting values of ΔV adopted in the literature, when defining samples of associated absorbers, are <3000 to <6000 km s^{-1}. ΔV is calculated as

$$\Delta V = c\frac{R^2 - 1}{R^2 + 1} \quad (1)$$

where c is the speed of light and

$$R \equiv \frac{1 + z_{abs}}{1 + z_{em}} \quad (2)$$

where z_{abs} and z_{em} are the absorption and emission redshifts, respectively. It is well known that the determination of QSO emission redshift is sensitive to the choice of emission lines (e.g. Gaskell 1982; Tytler & Fan 1992), where [O III] λλ 4959, 5007 is usually considered one of the most reliable indicators of systemic velocity. The SDSS composite spectrum of vanden Berk et al. (2001) shows that narrow forbidden lines may only be shifted by ± tens of km s^{-1}, but the commonly used Lyα, C IV and C III] lines may be offset by many hundred km s^{-1}. The majority of the PDLAs used in this study (see Section 2) are selected from the SDSS DR5 survey of Prochaska et al. (2008b), and we adopt their re-derived emission redshifts. For the QSOs not in the sample of Prochaska et al. (2008b) we derive emission redshifts in an identical way. The technique first calculates line centres of all significantly detected emission lines as described by Hennawi et al. (2006) and applies

[2]http://star-www.rl.ac.uk/star/docs/sun50.htx/sun50.html

[3]http://www.ucolick.org/~xavier/IDL

Table 2. PDLA redshifts and relative velocities.

QSO	log N(H I) (cm^{-2})	$z_{\rm em}$	$z_{\rm absH\,I}$	$z_{\rm absZ}$	$\Delta V_{\rm H\,I}$ (km s^{-1})	$\Delta V_{\rm Z}$ (km s^{-1})
J0140−0839	20.75 ± 0.15	3.7156 ± 0.012	3.6960	3.69660	1250	1211
J0142+0023	20.38 ± 0.05	3.3734 ± 0.008	3.34765	3.34768	1772	1769
Q0151+048	20.34 ± 0.02	1.9225 ± 0.003	1.9342	1.93429	−1199	−1208
J1131+6044	20.50 ± 0.15	2.9069 ± 0.009	2.8754	2.87562	2424	2412
J1240+1455	21.3 ± 0.2	3.1092 ± 0.005	3.1078	3.10803	102	85
J1604+3951	21.75 ± 0.2	3.1542 ± 0.007	3.1633	3.16711	−656	−930
J2321+1421	20.70 ± 0.05	2.5539 ± 0.006	2.5731	2.57312	−1616	−1618

the known systematic shifts of each species as tabulated by Shen et al. (2007) and Richards et al. (2002). The high ionization lines such as C IV and Si IV give the poorest estimate of $z_{\rm em}$, with a redshift error of ∼700 km s^{-1}. From the SDSS spectra, our best estimates of systemic redshift are derived from the Mg II emission line which yields $z_{\rm em}$ accurate to ∼270 km s^{-1}, based on the distribution of Mg II-[O III] offsets given in Richards et al. (2002). Emission redshift errors in Table 2 are based on the distributions of line shifts given in table 7 of Shen et al. (2007). For future studies, it would be desirable to obtain infrared (IR) spectra of these targets to obtain redshifts directly from the Balmer and forbidden [O III] lines (e.g. Rix et al. 2007), the latter of which yields accuracies of less than 50 km s^{-1}. Recently, Hennawi et al. (2009) have obtained an IR spectrum for one of our sightlines: J1240+1455, and for this object we adopt the emission redshift determined from the [O III] line ($z_{\rm em}$ = 3.1092). This value is larger by 160 km s^{-1} than the value derived from the SDSS spectrum ($z_{\rm em}$ = 3.1070) and is now larger than the absorption redshift.

Having made our best estimate of the emission redshifts of the QSOs in our sample, a value of the absorption redshift must also be obtained. The velocity spread of metal species in DLAs can extend over several hundred km s^{-1} (e.g. Prochaska et al. 2008a) and the redshift of the best-fitting Lyα line can be offset from the metals. In Table 2, we give the absorption redshifts of our sample determined from both the Lyα line and the strongest metal component ($z_{\rm absH\,I}$ and $z_{\rm absZ}$, respectively). It can be seen that the resulting difference in ΔV is much smaller than the typical error associated with the emission redshift determination. Since the Lyα redshift is the value most easily recovered from the literature, we adopt that as our fiducial measure of $z_{\rm abs}$.

4 COLUMN DENSITY MEASUREMENTS

For the three targets with UVES data, H I column densities were derived by fitting damped profiles to the Lyα absorption in the normalized spectra using the DIPSO software package. Continuum adjustment and H I fitting were carried out iteratively due to the proximity of the absorption line to the strong Lyα emission of the QSO itself. The H I column densities derived from the UVES data are all in good agreement with those derived from the SDSS spectra published in Prochaska et al. (2008b). Fig. 1 shows the Lyα fits to the PDLAs. For 2/3 of the UVES targets we were able to check our Lyα fits against an independent fit of Lyβ (for J0142+0023 Lyβ is blended with strong Lyα at a lower redshift). In both cases the Lyα and Lyβ column densities agree to within the errors quoted in Tables 1 and 2.

For the four HIRES targets where DLA fitting is hampered by the order-by-order normalization in XIDL, we adopt the H I column density derived from the SDSS spectrum (Prochaska et al. 2008b). As

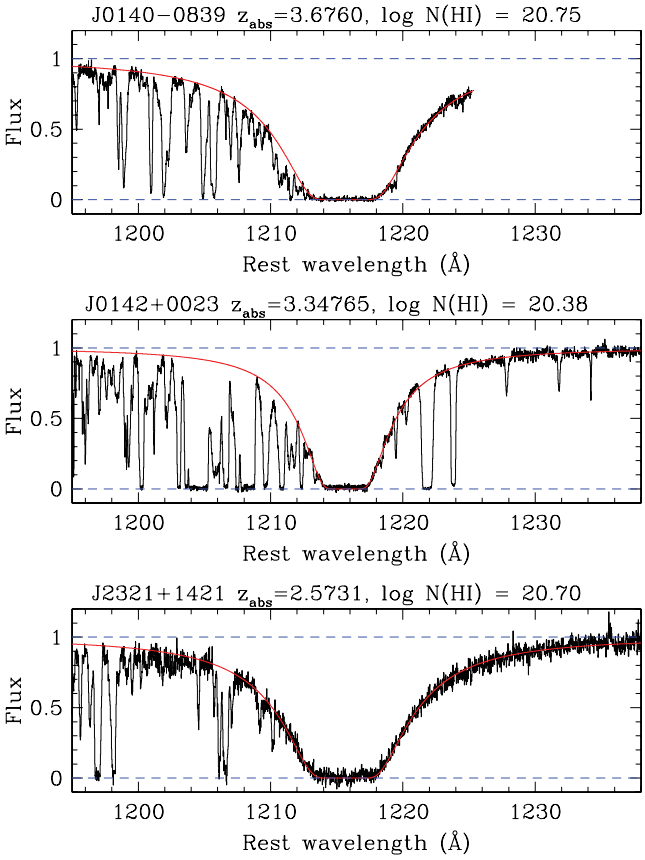

Figure 1. Fits to the Lyα profiles for the three PDLAs in our sample observed with UVES. Column densities and uncertainties are given in Table 1.

described above, the fits to the UVES spectra demonstrate that the SDSS values agree with the higher resolution spectra fits to within the errors. For Q0151+048, the H I column density was measured from an X-shooter spectrum by Zafar et al. (in preparation), which agrees with the value of Møller et al. (1998) to within 0.02 dex.

Metal column densities were mostly derived by fitting Voigt profiles with the VPFIT package.[4] The fitting of Voigt profiles is particularly useful in distinguishing contamination from blended absorption features and simultaneously fitting multiple transitions of a given species. In a few cases (noted below), usually when the line was too weak, or the S/N too low for a convincing Voigt profile decomposition, the apparent optical depth method (AODM; e.g. Savage & Sembach 1991) was applied. In general, the kinematic absorption model parametrized by redshifts and b-values (Doppler

[4]http://www.ast.cam.ac.uk/∼rfc/vpfit.html

Table 3. Column densities (in cm^{-2}) of low ionization species.

QSO	log N(Fe II)	log N(C II)	log N(Si II)	log N(S II)	log N(O I)	log N(Zn II)	log N(Cr II)	log N(N I)	log N(Al II)	log N(Ar I)
J0140−0839	<12.73	14.13 ± 0.08	13.51 ± 0.09	<13.33	14.69 ± 0.01	Blend	<12.39	<12.38	11.82 ± 0.04	<12.82
J0142+0023	13.7 ± 0.1	–	14.15 ± 0.03	13.28 ± 0.06	>15.01	<11.50	<12.17	Blend	12.73 ± 0.01	<12.57
Q0151+048	13.70 ± 0.01	>14.43	14.01 ± 0.05	<13.47	>14.84	<11.81	<12.45	13.06 ± 0.05	12.57 ± 0.05	–
J1131+6044	13.76 ± 0.03	>14.55	14.49 ± 0.13	< 13.29	>14.82	–	–	13.8 ± 0.15	–	<12.52
J1240+1455	14.60 ± 0.03	Sat/blend	15.93 ± 0.03	15.56 ± 0.02	>15.24	12.90 ± 0.07	<13.02	Blend	>13.56	–
J1604+3951	15.40 ± 0.15	>15.28	16.09 ± 0.02	15.70 ± 0.02	blend	13.0 ± 0.1	–	–	>14.00	yes/blend
J2321+1421	14.18 ± 0.03	>14.68	14.45 ± 0.04	<13.60	>15.10	<11.84	<12.57	13.64 ± 0.03	12.99 ± 0.02	<13.33

Table 4. Column densities (in cm^{-2}) of high ionization and excited species.

QSO	log N(C IV)	log N(Si IV)	log N(N V)	log N(O VI)	log N(Al III)	log N(C II*)
J0140−0839	<12.18	<12.20	<12.96	Blend	<11.52	<12.41
J0142+0023	14.25 ± 0.01	13.73 ± 0.01	<12.29	Blend	<12.4	–
Q0151+048	>14.50	13.75 ± 0.01	<12.66	–	12.3 ± 0.1	13.0 ± 0.2
J1131+6044	13.85 ± 0.05	13.33 ± 0.02	<12.68	Yes/blend	–	<12.51
J1240+1455	>15.13	>14.31	>14.86	–	Blend	Blend
J1604+3951	>15.05	>14.74	14.14 ± 0.02	Blend	13.44 ± 0.02	>14.30
J2321+1421	13.81 ± 0.05	13.37 ± 0.01	<12.62	Blend	<12.2	<12.55

widths) for multiple components were derived independently for each species. Again, exceptions to this are noted below, usually in cases where the lines are weak or blending is suspected. Tables 3 and 4 list the adopted column density for low and high ionization species, respectively.

The calculation of upper limits depends on an assumption of the number of pixels over which a line should be detected. For a line of given FWHM in Å, the observed frame n sigma equivalent width (EW) detection limit is given by

$$\mathrm{EW} = \frac{n \times \mathrm{FWHM}}{\mathrm{S/N}} \tag{3}$$

where S/N is the signal-to-noise ratio per pixel. In order to determine the appropriate value of the FWHM, we take the b-value of the strongest component of a detected species for a given line of sight (this is usually a transition of Si II or Fe II) and apply the correction $\mathrm{FWHM} = b \times 2\sqrt{\ln 2}$, before converting from km s^{-1} into Å. A single value of the FWHM is used for all low ions, C II* and Al III limits in a given sightline. Typical b-values are 4–8 km s^{-1}. If the strongest component is unresolved, a FWHM corresponding to the instrumental resolution is adopted, i.e. the FWHM that appears in equation (3) is the maximum of either the strongest component or the instrumental resolution. Had we assumed that the lines were unresolved rather than adopting true linewidths, the upper limits would have been underestimated by 0.2–0.3 dex. For C IV, Si IV and N V we assume a broader profile and adopt a single value of b = 10 km s^{-1}. Upper limits in this paper are quoted at 3σ significance.

For species where only saturated lines are detected, lower limit column densities have been derived by applying the AODM to the observed line with the lowest oscillator strength (f-value). Column densities are converted to abundances by adopting the solar scale of Asplund, Grevesse & Sauval (2005), with the exception of argon for which we adopt the improved value of Asplund et al. (2009). Meteoritic values are adopted with the exception of C, N and O where we take the photospheric values (and Ar where several indirect methods are used; see Asplund et al. 2009 for details). We note that there are significant differences in the solar abundances of some of these volatile elements relative to other commonly used reference scales (see e.g. Holweger 2001). All literature abundances used for comparison in the present work have therefore been re-calculated on the solar scale of Asplund et al. (2005). Following the standard procedure in DLA abundances, we assume that the singly ionized species dominate the total column densities [i.e. for element X, N(XII) = N(X)] and we do not apply ionization corrections. Even though this assumption may not hold in some of the PDLAs in our sample (we discuss ionization in Section 6), it is none the less of interest to apply this common practice to the PDLAs to assess its impact. Exceptions to this approximation are threefold for the elements reported from our data. Charge exchange reactions (and ionization potentials < 13.6 eV) keep the majority of nitrogen and oxygen in the neutral state and for aluminium both Al II and Al III can contribute significantly. Since we do not calculate ionization corrections on a system-by-system basis, aluminium is omitted in our final abundance listing (see Table 5).

Abundances are quoted relative to solar using the usual notation

$$[X/H] = \log\left[\frac{N(X)}{N(H)}\right] - \log\left[\frac{N(X)}{N(H)}\right]_{\odot}. \tag{4}$$

4.1 J0140−0839, log N(H I) = 20.75

The PDLA towards J0140−0839 has a simple velocity structure with two main components in the low ionization species at $v = 0$ and +50 km s^{-1} (see Fig. 2). Three unsaturated transitions of Si II are detected (λ_0 = 1260, 1304, 1526 Å), although the latter of these exhibits some blending. The column density is derived by fitting the two bluer transitions simultaneously in VPFIT. Ar I λ 1048 is blended but the redder transition (Ar I λ 1066) of the doublet coincides with a clean region of the spectrum and is used to determine an upper limit to the argon column density. Despite the fairly high S/N (30–50), Al II is barely detected and its column density is derived using both VPFIT and the AODM. In VPFIT we adopt the b-values and redshifts of the two strongest components of the Si II fit to derive log N(Al II) = 11.78±0.04. The AODM gives log N(Al II) = 11.85±0.14, in agreement with the fit, within the

Table 5. Abundances relative to the solar scale of Asplund et al. (2005), except for argon for which we use the value given in Asplund et al. (2009). The approximation of $N(\mathrm{X}) = N(\mathrm{XII})$ or $N(\mathrm{XI})$ has been assumed.

QSO	log N(H I)	[C/H]	[N/H]	[O/H]	[Si/H]	[S/H]	[Fe/H]	[Zn/H]	[Cr/H]	[Ar/H]
J0140−0839	20.75 ± 0.05	−3.01	< −4.15	−2.72	−2.75	< −2.58	< −3.47	–	< −1.99	< −2.33
J0142+0023	20.38 ± 0.05	–	–.	> −2.03	−1.74	−2.26	−2.13	< −1.49	< −1.84	< −2.21
Q0151+048	20.34 ± 0.02	> −2.30	−3.06	> −2.16	−1.84	< −2.03	−2.09	< −1.14	< −1.52	–
J1131+6044	20.50 ± 0.15	> −2.34	−2.48	> −2.34	−1.52	< −2.37	−2.19	–	–	< −2.38
J1240+1455	21.3 ± 0.2	–	–	> −2.72	−0.88	−0.90	−2.15	−1.01	< −1.91	–
J1604+3951	21.75 ± 0.2	> −2.86	–	–	−1.17	−1.21	−1.80	−1.36	–	–
J2321+1421	20.70 ± 0.05	> −2.41	−2.84	> −2.26	−1.76	< −2.26	−1.97	< −1.47	< −1.76	< −1.77

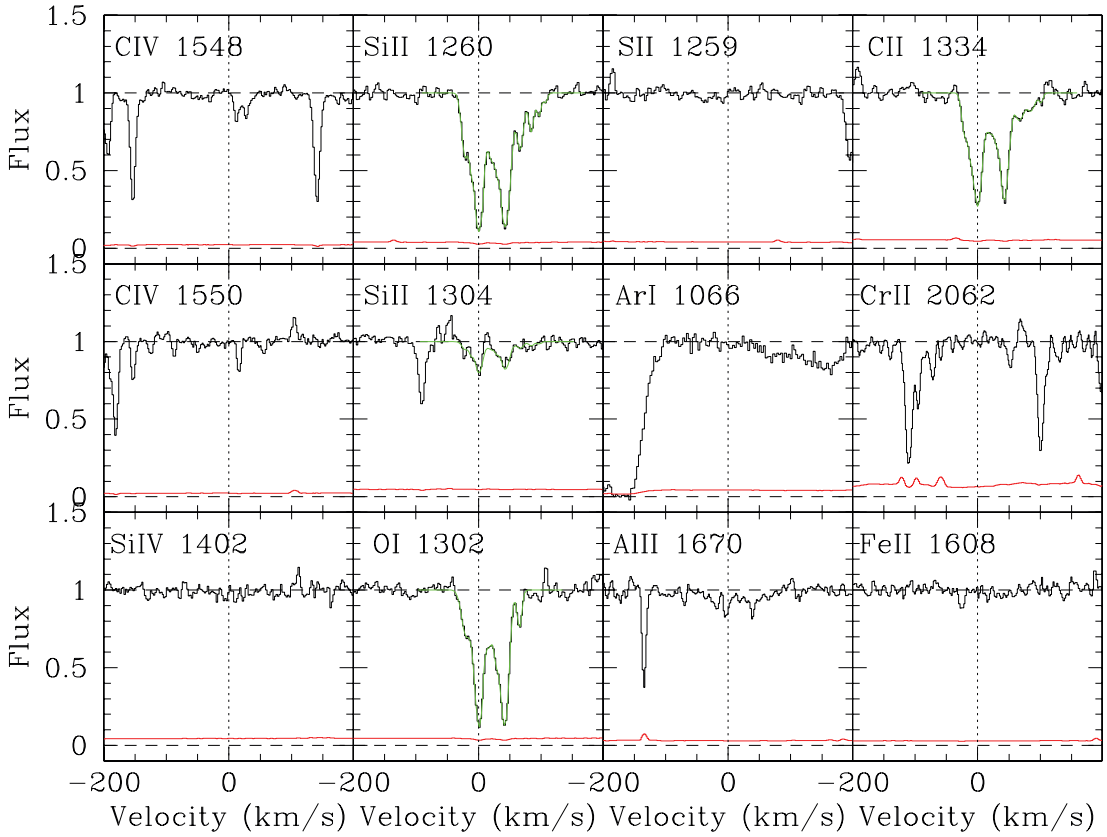

Figure 2. Selected metal line transitions in the PDLA towards J0140−0839. The lower solid (red) line shows the error array. When fits have been derived using VPFIT, those fits are overlaid in green. b-values for this absorber range from 2 to 8 km s^{-1}. Velocities are plotted relative to $z_{\mathrm{abs}} = 3.6966$.

errors. We adopt the average value of these two methods. No high ionization species were detected for this PDLA. C IV is usually detected even in the low metallicity Lyα forest (e.g. Cowie et al. 1995; Songaila 1997; Ellison et al. 1999, 2000), and at column densities of 1–3 orders of magnitude above our detection limit of $N(\mathrm{C\,IV}) < 12.18$. However, this PDLA is extremely metal-poor; both its Si and Fe abundances are the lowest in the current published literature (of which we are aware). Fox et al. (2007) have shown that there is a broad correlation between N(C IV) and metallicity, consistent with the non-detection of C IV in this PDLA. As we discuss in Section 6, there may be corrections due to ionization effects (and additionally some dust depletion, at least in the case of Fe). However, the O I is little affected by dust and ionization and the O I λ 1302 line is unsaturated in this PDLA, from which we determine [O/H] = −2.72. This supports an intrinsically low metallicity for this system. Indeed, the [O/H] of this PDLA is similar to the oxygen abundance of the IGM (Simcoe, Sargent & Rauch 2004; Aguirre et al. 2008) who find [O/H] ∼ −2.5 to −3 depending on the local overdensity, although this depends on the model for ionization corrections and shape of the UV background. Previously, a metallicity 'floor' has been suggested for DLAs (e.g. Prochaska et al. 2003a) and this system offers a rare chance to measure abundances at extremely low levels of enrichment. For example, Akerman et al. (2005) and Pettini et al. (2008) discuss how carbon abundances at low metallicity might provide clues into the yields of early stellar populations. The unsaturated C II λ 1334 yields [C/O] = −0.29 supporting the idea of an upturn in C/O ratios at low (O/H) (Pettini et al. 2008). The non-detection of N also sets a very low upper limit to N/O: [N/O] < −1.43.

4.2 J0142+0023, log N(H I) = 20.38

Selected metal lines are shown in Fig. 3. Two lines of Si II (λ 1304 and λ 1526) are detected, although they are approaching saturation.

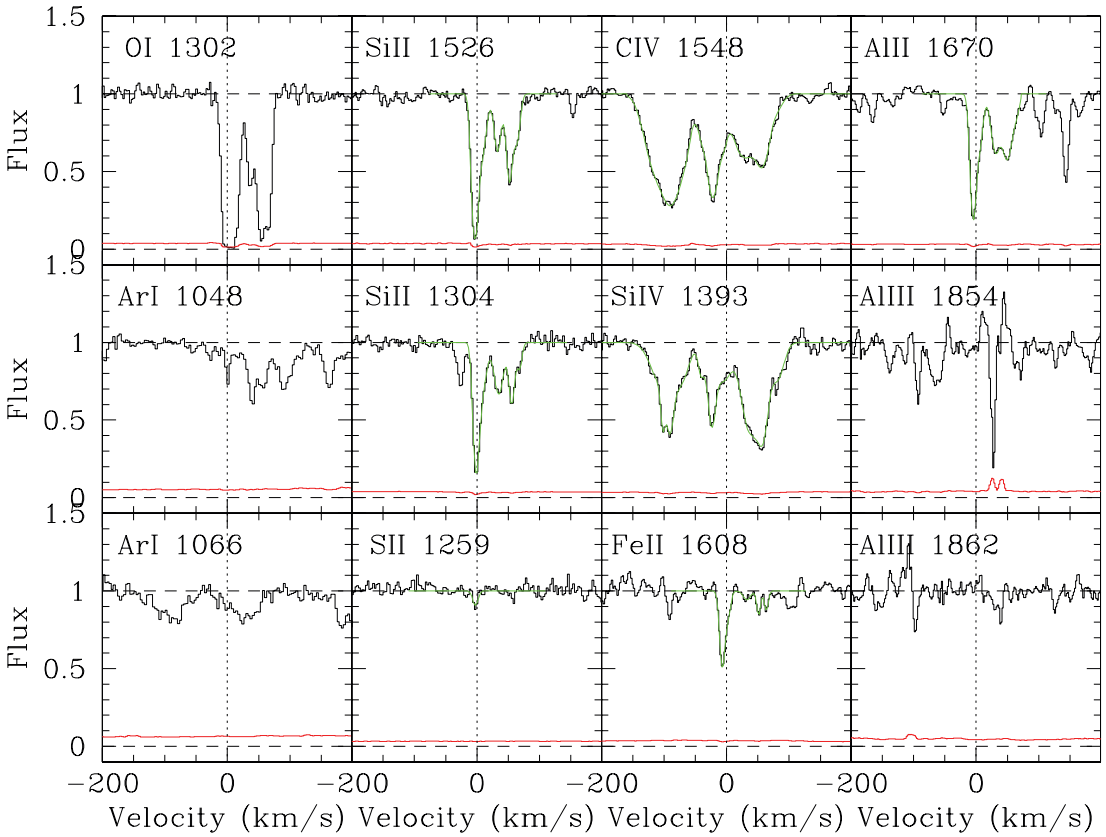

Figure 3. Selected metal line transitions in the PDLA towards J0142+0023. The lower solid (red) line shows the error array. When fits have been derived using VPFIT, those fits are overlaid in green. *b*-values for this absorber range from 3 to 9 km s^{-1} for the low ionization species and 7 to 25 km s^{-1} for the higher ionization species. Velocities are plotted relative to $z_{\rm abs} = 3.3477$.

N(Si II) was obtained separately for the two transitions with VPFIT and found to be in excellent agreement. Al II λ 1670 follows the velocity structure of the other low ions. There is weak absorption at Al III λ 1862 at a similar velocity, although gas in a different ionization state need not necessarily trace the neutral gas. A comparison with Al III λ 1854 could confirm the detection, but unfortunately this line is blended, so the detection of the λ 1862 line remains uncertain. We therefore calculate N(Al III) from Al III λ1862 and take this as an upper limit. S II λ 1259, although weak, is statistically a 5σ detection. Absorption is detected from both Si IV and C IV. Absorption is present in a similar velocity range as the low ions, but with additional components present at negative velocities from −150 to 0 km s^{-1}. There is a significantly detected feature at the expected velocity of Ar I λ 1048, but additional absorption extending to larger velocities alerts us to the possibility of contamination. The identification of this line as Ar I λ 1048 could be confirmed by the simultaneous detection of Ar I λ 1066, but this line is blended with Lyα. Assuming the $v = 0$ feature is Ar I λ 1048, we derive a column density from the AODM and quote this as a conservative upper limit.

4.3 Q0151+048, log N(H I) = 20.34

Selected metal lines for the PDLA towards Q0151+048 are shown in Figs 4 and 5. As described by Møller et al. (1998), Fynbo, Møller & Warren (1999) and Fynbo, Burud & Møller (2000), Q0151+048 has a close, but fainter, companion, Q0151+048B, which is separated by 3.27 arcsec (∼27.5 h_{70}^{-1} kpc). Møller et al. (1998) give the redshift of Q0151+048 to be $z_{\rm em} = 1.922 \pm 0.003$ and a slightly higher value for Q0151+048B of $z_{\rm em} = 1.937 \pm 0.005$. As shown by Zafar et al. (in preparation) Q0151+048B shows no DLA absorption, despite its relatively small transverse separation. Using the same technique described in Section 3, we re-evaluate the redshift of Q0151+048 and Q0151+048B from X-shooter spectra kindly provided by Johan Fynbo and Tayyaba Zafar. We determine $z_{\rm em} = 1.9225 \pm 0.003$ for Q0151+048 and $z_{\rm em} = 1.9237 \pm 0.003$ for Q0151+048B, where both redshifts are based on the Mg II line. However, we caution that the spectrum of Q0151+048B is affected by a lot of structure in the continuum shape which may compromise the accuracy of the redshift (the quoted error only accounts for known systematic offsets of emission lines from the systemic value). Interestingly, the PDLA studied by Rix et al. (2007) towards Q2343−415 also has a nearby QSO companion (Q2343+125) separated by 680 h_{70}^{-1} kpc and −100 km s^{-1}.

N(Fe II) is derived from a simultaneous VPFIT of Fe II λ 1608 and Fe II λ 1144. Similarly, N(Si II) is determined by simultaneously fitting the lines at λ 1304 and 1526 Å. The N I column density was determined from a simultaneous fit of N I λ 1199 and N I λ 1200.2. C II* is detected, but its low optical depth precludes an accurate Voigt profile fit; its column density is derived from the AODM. By combining N(C II*) with N(H I) it is possible to determine the cooling rate, $l_{\rm c}$, which Wolfe et al. (2008) have recently shown to be bi-modal. We calculate a cooling rate log $l_{\rm c} = -26.86$ which qualifies this PDLA as a 'high cool' (i.e. high cooling rate) system. Such systems typically have higher metallicities, dust-to-gas ratios and velocity spreads than the low cooling rate DLAs. However, the PDLA towards Q0151+048 has a relatively narrow velocity structure and apparently low metallicity ([S/H] ≤ −2.03). Either

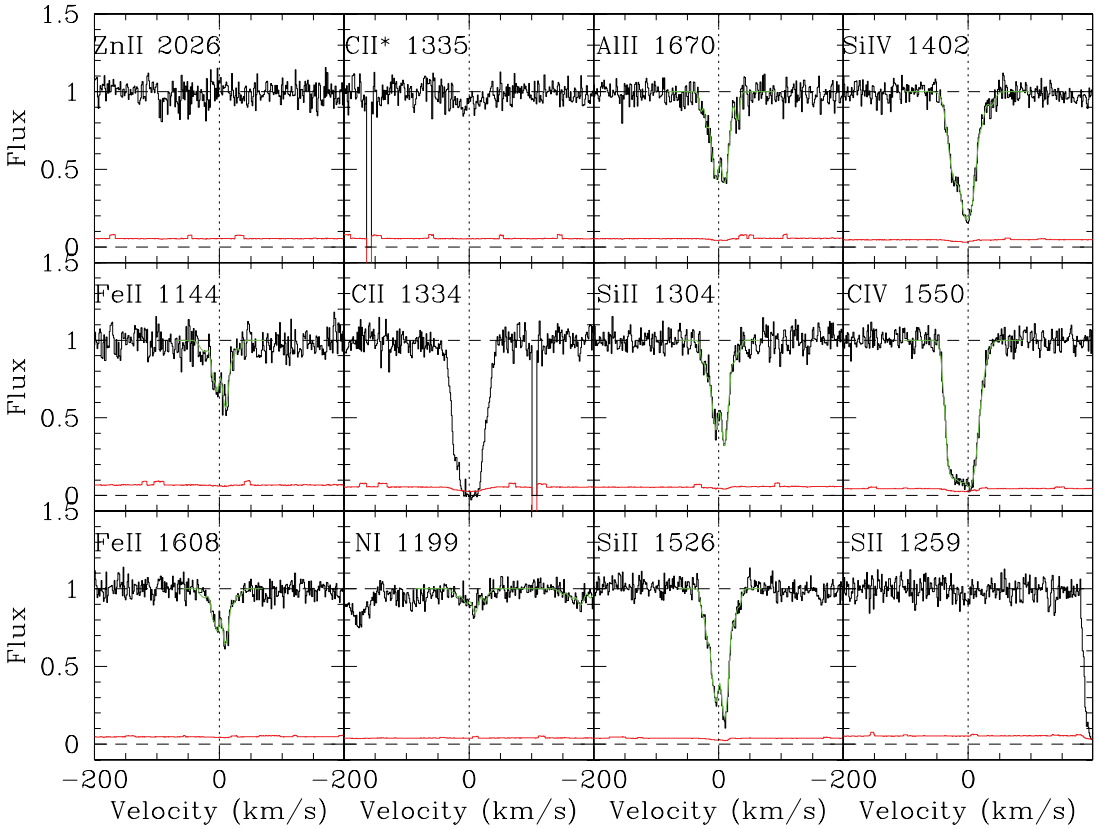

Figure 4. Selected metal line transitions in the PDLA towards Q0151+048. The lower solid (red) line shows the error array. When fits have been derived using VPFIT, those fits are overlaid in green. *b*-values for this absorber range from 2 to 8 km s^{-1} for the low ionization species and 5 to 15 km s^{-1} for the higher ionization species. Velocities are plotted relative to $z_{\rm abs} = 1.9342$.

this PDLA is rather unusual amongst the 'high cool' population, or the column densities may be affected by ionization. However, it should be noted that it lies towards the lower end of the $l_{\rm c}$ distribution for high cool systems. The low N(H I) of this system makes the latter possibility a likely explanation and we present more evidence for ionization in low N(H I) PDLAs in Section 6.

Both C IV and Si IV are very strong and may be partly saturated. The velocity structure is simple and coincides with that of the low ions (see Fig. 4), which is usually not the case for intervening DLAs. AODM and VPFIT give consistent lower limits for C IV. N(Si IV) is derived from the λ 1402 line due to mild saturation in the bluer member of the doublet. In Section 6, we discuss the relative contributions of Si II and Si IV in this PDLA and the implications of coincident velocity structure.

Although no N V is found at the redshift of the main absorber, there is N V offset by ~ -825 km s^{-1}. This velocity corresponds to a redshift that is well offset into the Lyα wing (see Fig. 5), and does not appear to be associated with high column density H I. The N V is well-fit in VPFIT (Fig. 5); so there is no evidence for partial coverage in the current data. The N V is accompanied by weak C IV, but no Si IV (O VI is not covered by the spectra). The column densities of this component are not included in the main table (Table 5) as this absorption does not appear to be associated with the same PDLA system. From VPFIT we determine N(N V) = 13.12±0.03 from the λλ 1238, 1242 doublet and N(C IV) = 12.89±0.02. This offset absorption is qualitatively similar to the intervening systems studied by Schaye, Carswell & Kim (2007), who describe a population of absorbers with significant column densities of C IV and N V, but with little H I. Weidinger et al. (2005) also find orphaned N V near a proximate Lyman limit system with even larger velocity offset. Fechner & Richter (2009) give the line of sight number density of intervening N V absorbers to be dN/dz = 1.16. For a $\Delta z = \pm 0.01 = 0.02$ (which corresponds to $\pm \sim 1000$ km s^{-1} at $z = 2$) there is a 0.2 per cent random chance that an intervening N V system lies this close to a PDLA. We discuss the offset N V further in Section 9.

4.4 J1131+6044, log N(H I) = 20.50

Selected metal line transitions for the PDLA towards J1131+6044 are shown in Fig. 6. The Si II column density is determined solely from the λ 1526 line due to saturation of Si II λ 1260, blending of the Si II λ 1304 line and no coverage of Si II λ 1808. Similarly, the only detected Fe II line is at $\lambda_0 = 1608$ Å. Fixing the velocity structure to match that of the Si II fit produces an excellent fit. Of the N I triplet, only the bluest transition at $\lambda_0 = 1199$ Å is unblended. We determine N(N I) using both the fixed component model derived from Si II and a free fit. The former produces a relatively poor fit (but does not indicate Lyα blending) to the data and yields N(N I) = 13.87 ± 0.09. The latter yields a slightly lower N(N I)=13.76 ± 0.08. We adopt an intermediate value of 13.8 ± 0.15. There is a weak (5σ) feature at the expected position of Ar I 1048 whose column density can be determined from the AODM. Ideally, the detection of Ar I λ is required to confirm that this is not contamination by weak Lyα. However, since Ar I λ 1066 is not detected to confirm

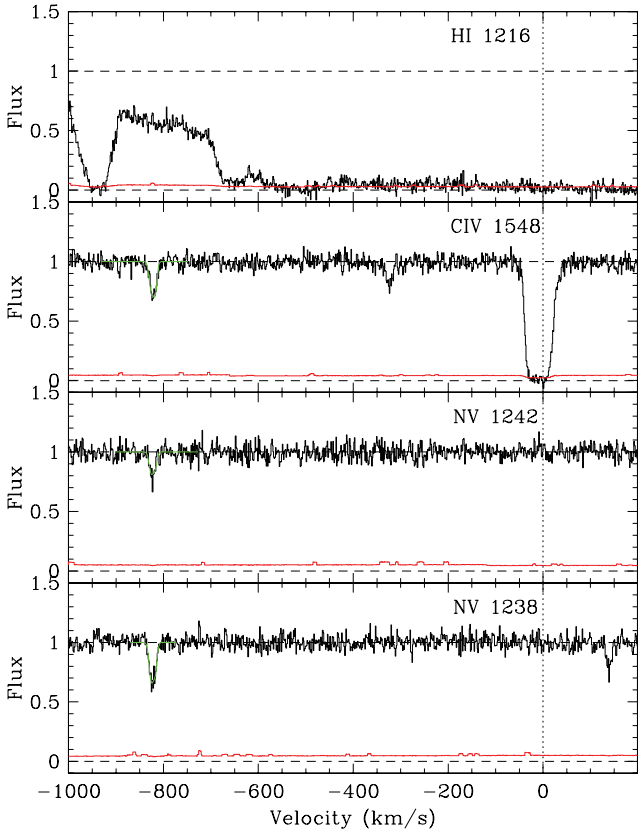

Figure 5. Highly offset N v and C iv in the PDLA towards Q0151+048. The lower solid (red) line shows the error array. When fits have been derived using VPFIT, those fits are overlaid in green. Velocities are plotted relative to $z_{\rm abs} = 1.9342$.

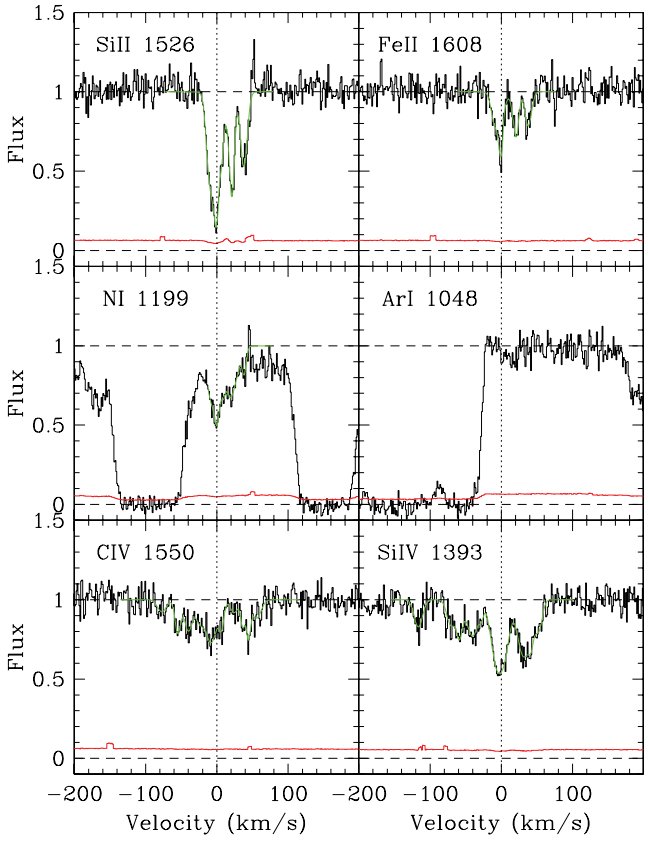

Figure 6. Selected metal line transitions in the PDLA towards J1131+6044. The lower solid (red) line shows the error array. *b*-values for this absorber range from 2 to 8 km s^{-1} for the low ionization species and 2 to 10 km s^{-1} for the higher ionization species. When fits have been derived using VPFIT, those fits are overlaid in green. Velocities are plotted relative to $z_{\rm abs} = 2.87562$.

the identification, we take the conservative approach and use the AODM-derived column density as a limit.

Although this PDLA has a relatively high ΔV (~ 2400 km s^{-1}) it still demonstrates some interesting properties, most notably in its high ionization lines. At $v \sim 0$ the C iv and Si iv absorption is relatively weak. The Si iv λλ 1393, 1402 doublet is fitted simultaneously. The C iv λ1548 line is blended with extended negative velocity gas (see below and Fig. 7) so N(C iv) is determined solely from C iv λ 1550. There is no N v at $v = 0$ but we are not able to determine whether or not O vi is present due to the blending in at least one of the doublet components. However, the kinematic similarity between absorption at the expected wavelength of O vi λ 1031 and C iv λ 1550 is suggestive (Fig. 7). We do find highly offset absorption of strong C iv and O vi (but no N v) at $v \sim -750$ km s^{-1}. Since we cannot estimate the total O vi column density due to blending, no value is given in Table 4. The C iv extends[5] from approximately -500 to -1150 km s^{-1}. We cannot confirm the full extent of the O vi in velocity space due to various Lyα blends (see Fig. 7). The metal column densities in this extended component are not included in the values in Table 4.

[5]There are two weakly detected features in this approximate velocity range that could be N v λ1238. However, N v λ 1242 is not detected at these extended velocities, so these identifications cannot be confirmed with the present data.

4.5 J1240+1455, log N(H i) = 21.3

Selected metal lines are shown for the PDLA towards J1240+1455 in Fig. 8. This PDLA was studied by Hennawi et al. (2009) using the original SDSS spectrum. Like several other PDLAs (Møller & Warren 1993; Møller et al. 1998; Leibundgut & Robertson 1999; Ellison et al. 2002), this absorber has Lyα emission superimposed in the DLA trough. After extensive modelling, Hennawi et al. (2009) concluded that the Lyα emission is likely to be associated with the QSO, and not the PDLA itself.

This is a relatively faint QSO and the HIRES spectrum exhibits a low S/N. None the less, we are able to detect a number of metal lines due to the high N(H i) (see Fig. 8). For example, all three lines in the S ii λλλ 1250, 1253, 1259 triplet are detected and are fitted simultaneously. We check for saturation by additionally calculating the AODM column densities, which yield the same column density in each triplet. Due to the low S/N, we determine N(Fe ii, Si ii) in three different ways: using a fixed component VPFIT model based on the component structure of S ii, a model where the component structure can vary and finally the AODM. All give very consistent answers, so we adopt that of the fixed component VPFIT model. Since the optical depths in the line centres of the Si ii and Fe ii lines are less than in the demonstrably unsaturated S ii lines, saturation does not seem to be an issue. The Fe and Cr abundances are both low in this system (e.g. relative to Zn), indicating that dust depletion may be significant. Strong, broad N v absorption is detected offset by

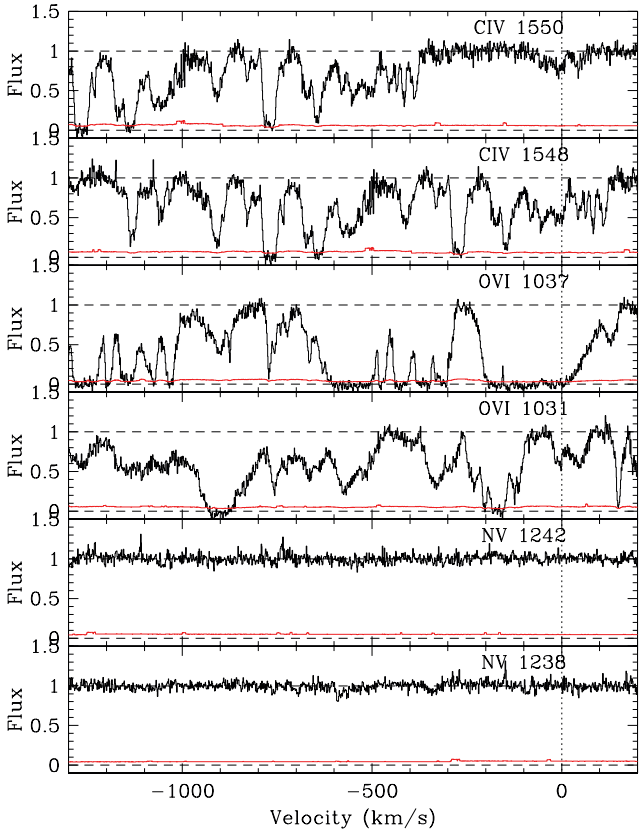

Figure 7. C IV, O VI and N V coverage in the PDLA towards J1131+6044 over an extended velocity scale. The lower solid (red) line shows the error array. O VI is detected at $v \sim -750$ km s^{-1} and C IV is present from -1150 to approximately -500 km s^{-1}. There is no definitive detection of N V. Velocities are plotted relative to $z_{\rm abs} = 2.87562$.

~ -120 km s^{-1} from the strongest low ion component. Only the weaker N V λ 1242 line is fitted, although even this may be partly affected by saturation. We therefore conservatively quote the fit as a lower limit in Table 4. C IV and Si IV are both heavily saturated and C II* is blended.

4.6 J1604+3951, log N(H I) = 21.75

The PDLA towards J1604+3951 exhibits two main components in the low ionization gas separated by about 250 km s^{-1} (see Fig. 9). However, the strongest transitions, such as C II λ 1334 and Al II λ 1670, show almost continuous absorption over 600 km s^{-1}. Singly and multiply ionized species exhibit quite similar velocity structure, e.g. Si II and Si IV (Fig. 10). In the α elements (Si and S) the redder component is stronger, but in Fe-peak (Fe and Ni) the blue component is stronger. The absorption structure of Zn II is more akin to Si and S than Fe and Ni, even though it is often considered to track the Fe-peak. We return to this point in the following text.

S II λ 1250 and λ 1253 are fitted simultaneously and we apply the same model for Si II λ 1808. Fe II λ1608 is saturated in several components and yields a lower limit of N(Fe II) > 15.15. Fortunately, Fe II λ1611 is detected, albeit with low optical depth. We try both a fixed (tied to the S II structure) and free velocity model; both give a consistent answer of N(Fe II) = 15.35 ± 0.03. The AODM gives a slightly higher value of N(Fe II)=15.45 ± 0.2. We adopt an intermediate value of N(Fe II) = 15.4 ± 0.15. C II*λ1335 is saturated at $v \sim 0$ km s^{-1} and the negative velocity component is blended with C II λ1334. We therefore quote a lower limit that is very conservative since it does not (cannot) account for the negative velocity gas. Saturation and blending mean that the lower limit for C II λ 1334 is similarly conservative. As for Fe II, we attempt three different approaches for Zn, all give consistent values, so an average is taken. Ar I λ 1048 is blended, as are the weaker components of Ar I λ 1066. However, the strongest velocity component of Ar I λ 1066 appears clean. Whilst it is therefore not possible to report a total N(Ar I), we fit the Ar I λ 1066 line with the same velocity structure as Si II to derive N(Ar I) = 14.45 for the $v = 0$ complex. The Si II column density for these components is 15.96, yielding [Ar/Si] = −0.40.

Fig. 10 shows absorption from the more highly ionized species. C IV and Si IV are particularly strong. Due to the wide velocity structure, C IV is self-blended. The limit for N(C IV) is therefore derived from the blue (negative velocity) component of C IV λ1548. N V is detected, but the poor continuum determination makes fitting Voigt profiles challenging. A simultaneous fit to N V λ1238 plus N V λ 1242 from −100 to 250 km s^{-1} yields N(N V) = 14.14 ± 0.02 (the error does not include errors in the continuum). There appears to be further N V at −400 km s^{-1}, where C IV and Si IV are also seen, but not the low ionization species. Fits to this bluer component are hampered by the poor continuum placement and possible blending from other lines and not accounted for in the column density quoted in Table 4.

Considering the relative abundances yields some clues to the difference in the velocity structure of the low ions. The column densities for the two main velocity components at −240 and 0 km s^{-1} are given in Table 6. Also tabulated are the relative abundances of some key elemental ratios. Both components have [S/Si] ratios consistent with the solar value, as expected from studies of Galactic stars (Chen et al. 2002). Similarly, the [S/Zn] ratio is consistent with mild α element enhancement in both components (where S and Zn are both undepleted and therefore a useful combination for this assessment; see e.g. Nissen et al. 2004). However, whereas the blue component has a solar [Zn/Fe] ratio, the gas at $v \sim 0$ km s^{-1} has a very high value: [Zn/Fe] = 0.75. These results are strongly indicative of depletion patterns varying within the galaxy.

There is a possible detection of Si II*λ 1264. Although excited transitions of Si and Fe have been previously reported in DLAs associated with GRBs (e.g. Prochaska, Chen & Bloom 2006; Vreeswijk et al. 2007), this is the first possible detection in a QSO (P)DLA. The fit gives N(Si II*) = 12.6 ± 0.1. Although this column density is 16 times larger than the 3σ upper limit derived for the absorber PKS 1443+27 (Howk, Wolfe & Prochaska 2005), the N(H I) of the PDLA is also almost 10 times higher. Unfortunately, the saturation of the C II* transition precludes an estimate of the warm neutral medium fraction in this absorber.

4.7 J2321+1421, log N(H I) = 20.70

The PDLA towards J2321+1421 has a relatively simple velocity structure with most of the absorption centred within ±40 km s^{-1} of $z_{\rm abs} = 2.5731$ (see Fig. 11). N(Fe II) is determined from a simultaneous fit to Fe II λ 1608 and Fe II λ 2374, both of which are unsaturated. Si II λ 1808 is a marginal detection, whereas Si II λ 1304 and Si II λ 1526 are mildly saturated. None the less, combining the three transitions we are able to constrain the total Si II column density. The region of spectrum around the strongest Cr II line at $\lambda_0 = 2056$ Å is relatively noisy, so we derive an upper limit from the non-detection of Cr II λ 2062. There is minor blending of N I with Lyα forest lines but simultaneous fitting of the triplet gives a consistent fit. There

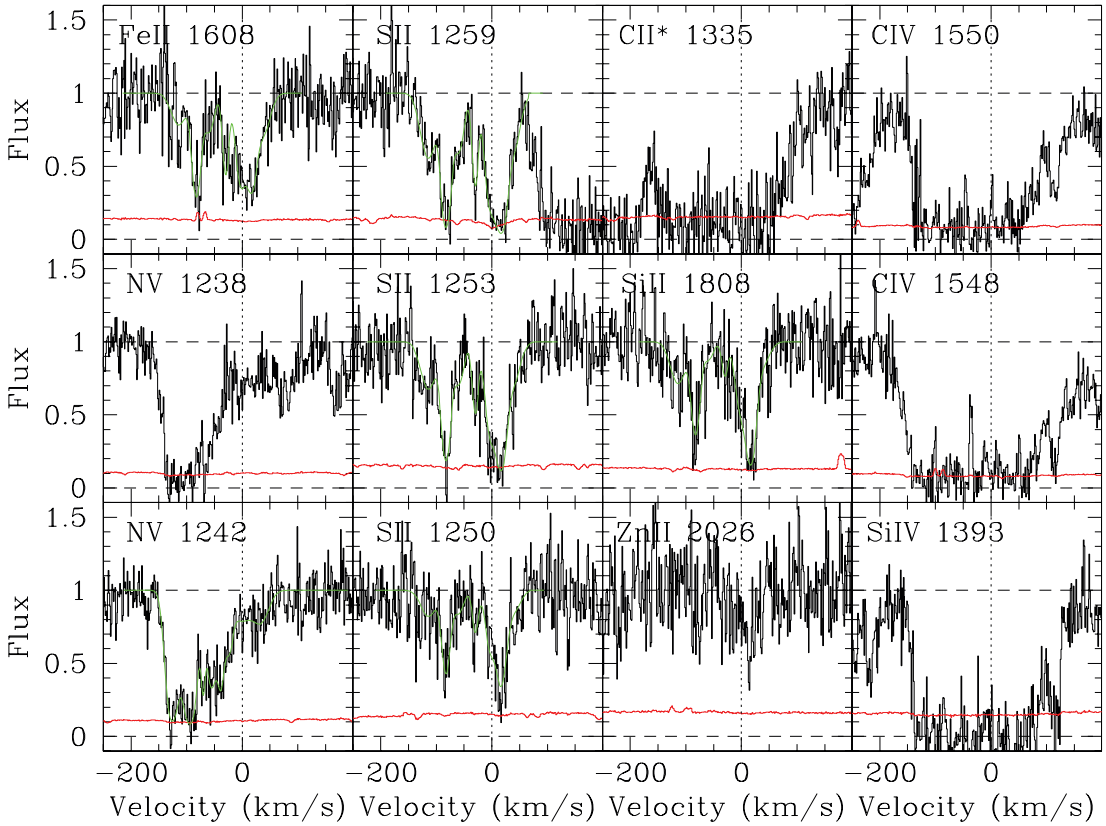

Figure 8. Selected metal line transitions in the PDLA towards J1240+1455. The lower solid (red) line shows the error array. When fits have been derived using VPFIT, those fits are overlaid in green. *b*-values for this absorber range from 7 to 18 km s^{-1} for the low ionization species and 6 to 30 km s^{-1} for the higher ionization species. Velocities are plotted relative to $z_{\rm abs} = 3.1078$.

is weak (6σ) absorption at approximately the expected position of Al III λ 1854; N(Al III) = 12.2 is determined from the AODM. However, this is inconsistent with the non-detection of Al III 1862 for which we derive a 3σ limit of N(Al III) <11.9. Given the weakness of the 1854 Å line and the possibility of contamination we give 12.2 as a conservative upper limit. C IV and Si IV are detected, but offset by -100 km s^{-1} from the strongest low ion absorption, but coincident with much weaker column density components e.g. in Al II and Fe II (see Fig. 11). The spectral region around the Ar I doublet is fairly noisy. Ar I λ 1066 is not detected, but there is a 5σ feature at the expected velocity of Ar I λ 1048. However, the S/N at this wavelength is only around 2 per pixel, so we consider this unreliable and therefore conservatively adopt the upper limit from Ar I λ 1066.

5 ADDITIONAL PROXIMATE AND INTERVENING DLAS FROM THE LITERATURE

Although the work presented here represents the first systematic study of a sample of PDLAs, a small number of proximate systems have been included in literature studies of intervening absorbers. In this section, we search the literature for PDLAs that meet our ΔV selection criterion and with measured metal column densities that can be used to enlarge our sample. We also describe the compilation of a comparison sample of intervening DLAs with which the PDLAs can be compared.

5.1 PDLAs in the literature

We searched for additional PDLAs with known abundances by trawling the catalogue of Dessauges-Zavadsky et al. (in preparation). Emission redshifts were taken from the references given in Dessauges-Zavadsky et al. (in preparation); if no emission redshift was present in the referenced paper, we used SIMBAD. Due to the numerous different techniques and inherent uncertainties in emission redshift determination, a first cut was made for literature DLAs with $\Delta V < 5000$ km s^{-1}, of which there are 15 in the Dessauges-Zavadsky catalogue. We obtained literature spectra for 14/15 of these targets that were suitable for a re-assessment[6] of $z_{\rm em}$ using the technique described in Section 3. In this way, all of the PDLA emission redshifts and hence the ΔV-values are computed in a consistent way. In Table 7, we list the PDLA candidates selected from the literature together with updated emission redshifts and re-computed ΔV where available. There is no obvious trend of $\Delta V_{\rm new} - \Delta V_{\rm old}$ with redshift, and positive and negative changes are present in approximately equal number. Only one QSO's redshift changes by > 1000 km s^{-1}, namely Q0425−5214 (CTS 436) whose redshift is obtained from the Lyα line (Maza et al. 1995). Not only is this line a poor indicator of systemic redshift, but the spectrum is of very low dispersion (30 Å resolution), but Maza et al. (1995) also report redshifts as being accurate to only ±0.02. We discard absorbers with $\Delta V > 3000$ km s^{-1}.

[6]We were unable to locate a suitable spectrum for the re-measurement of the emission redshift of Q0201+365.

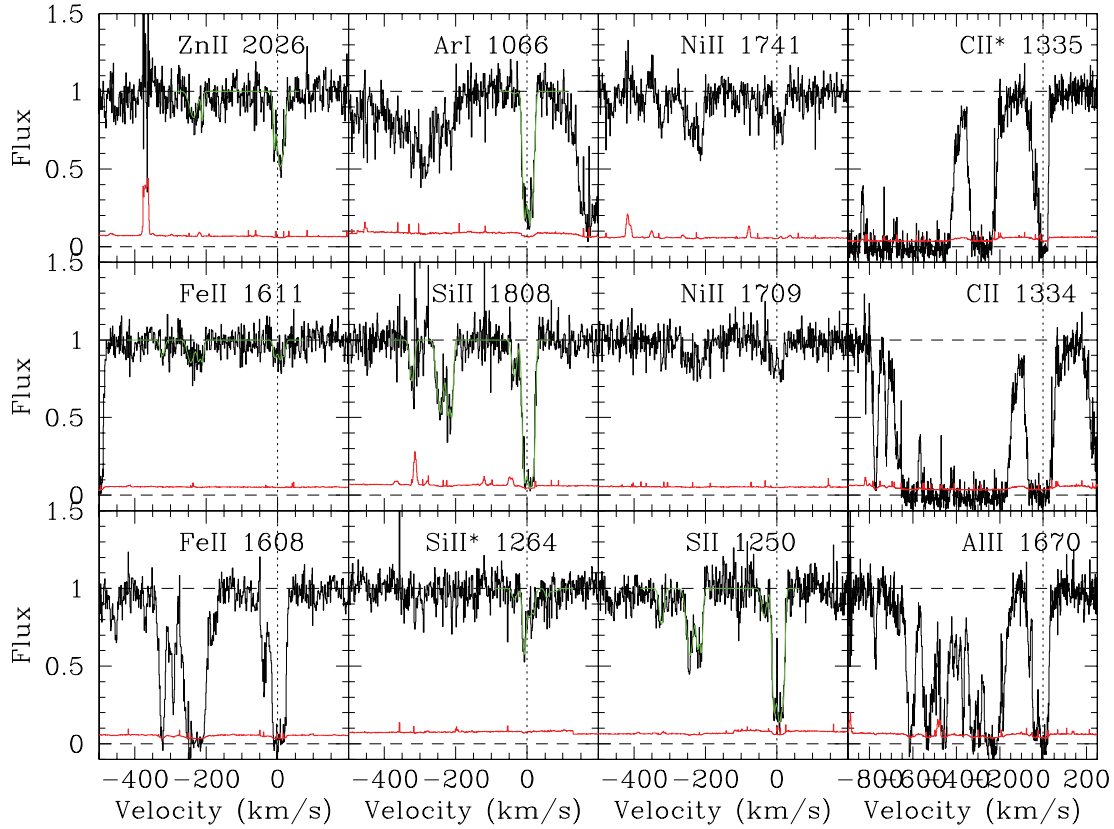

Figure 9. Low ionization metal line transitions in the PDLA towards J1604+3951. The lower solid (red) line shows the error array. When fits have been derived using VPFIT, those fits are overlaid in green. *b*-values for this absorber range from 3 to 12 km s^{-1} for the low ionization species. Velocities are plotted relative to $z_{\rm abs} = 3.1670$. Note the different velocity scale of the last column. The C II* line is blended to the blue with C II.

To complement the abundances determined for our new data sample (Section 4), column densities for literature PDLAs with $\Delta V <$ 3000 km s^{-1} are taken from Dessauges-Zavadsky et al. (in preparation) and combined with our new echelle sample. The final PDLA sample therefore contains 7+9 (new plus literature, respectively) PDLAs.

In addition to the column densities available in the literature (Table 8) we determine the column density of S II towards J2340−00 from the extant HIRES spectrum. All three transitions in the S II triplet at λλλ 1250, 1253, 1259 Å are well detected. We determine the column densities using the AODM and find that all three lines yield values in excellent agreement.

5.2 DLA comparison sample

To compare the PDLAs with intervening DLAs we used the sample of Dessauges-Zavadsky et al. (in preparation). In order to circumvent the large uncertainties in ΔV incurred through $z_{\rm em}$ measurements, we impose a lower limit of 10 000 km s^{-1} which yields a sample of 180 intervening DLAs with log N(H I) $\geq$ 20.3 from the Dessauges-Zavadsky catalogue. We adopt the column density measurements compiled by Dessauges-Zavadsky et al., and convert to abundances using the same solar scale that was applied to the PDLAs (Asplund et al. 2005). In Sections 6 and 7, we compare the properties of the PDLAs with the DLAs in order to gain insight into whether they represent similar populations and what the effect of QSO proximity is.

6 IONIZATION

The proximity of PDLAs to their background QSO naturally leads to the question of whether they are strongly affected by the quasar's intense ionizing radiation. Thus far, there are conflicting indications in the literature for studies of individual systems. Rix et al. (2007), in their detailed study of a single PDLA towards Q2343−BX415, concluded that ionization corrections were small. None the less, they identify absorption from highly ionized species such as N V which are relatively rarely detected in intervening absorbers and require high energy photons if produced via photoionization. One of the PDLAs in our sample (J1240+1455) has previously been reported to exhibit N V in the low-resolution SDSS spectrum (Hennawi et al. 2009) which we confirm in our echelle spectra (see Section 4.5). Fox et al. (2009) find that ∼13 per cent of intervening systems also exhibit N V and do not find any increase in its incidence in PDLAs with relative velocities 500 $< \Delta V <$ 5000 km s^{-1} relative to the intervening systems at $\Delta V >$ 5000 km s^{-1}. In a general survey of N V at all N(H I) column densities, Fechner & Richter (2009) do find a proximate excess, a conflict which appears to be linked to the velocity range used (see discussion below). Finally, Lyα emission in the DLA trough has been found for several PDLAs (Møller & Warren 1993; Møller et al. 1998; Leibundgut & Robertson 1999; Ellison et al. 2002; Hennawi et al. 2009), a feature which is much rarer amongst the intervening DLA population. In this section, we assess various indications of ionization in the sample of 16 PDLAs, paying special attention to elements which might indicate ionization by a hard radiation source, as might be expected from the proximity to the QSO.

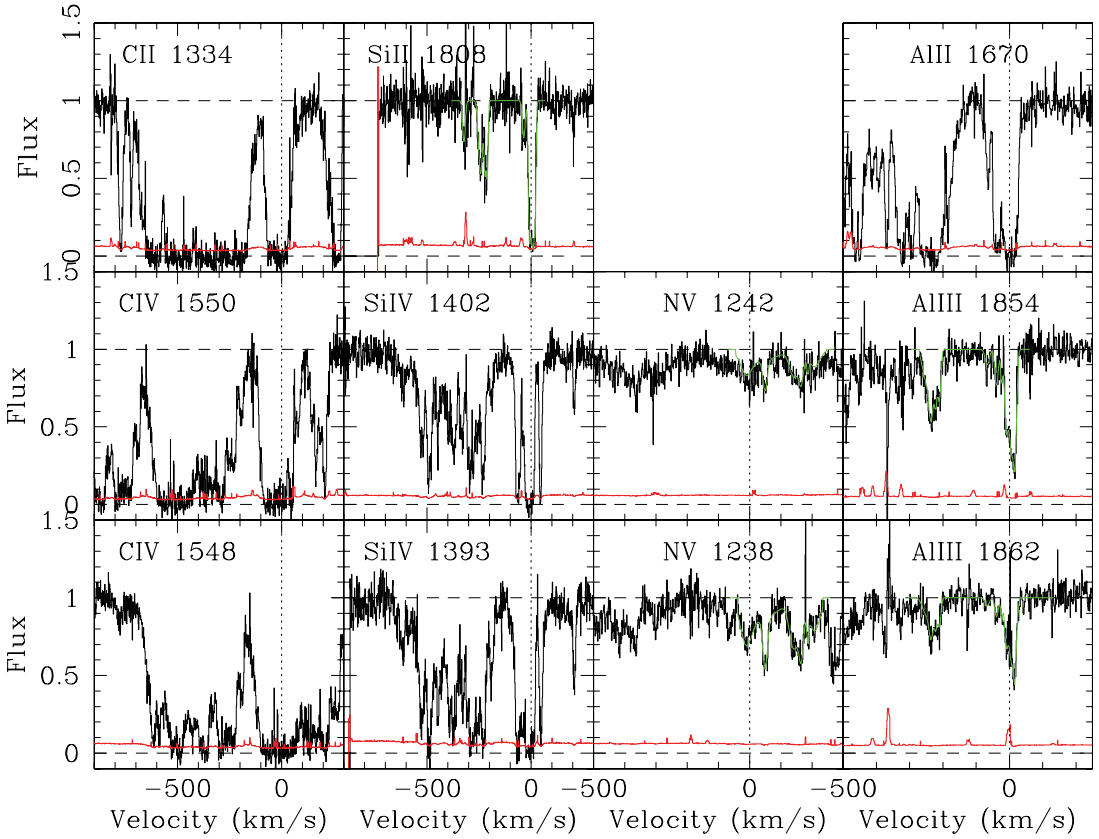

Figure 10. High ionization metal line transitions in the PDLA towards J1604+3951. The lower solid (red) line shows the error array. When fits have been derived using VPFIT, those fits are overlaid in green. *b*-values for this absorber range from 3 to 25 km s^{-1} for the high ionization species. Velocities are plotted relative to $z_{\rm abs} = 3.1670$. The red component of C IV 1548 is blended with the blue component of C IV 1550. The upper row shows some of the low ions (repeated from Fig. 9) for comparison.

Table 6. Column densities (cm^{-2}) and abundance ratios in two components in PDLA J1604+3951.

	Blue cpt. $v \sim -240$ km s^{-1}	Red cpt. $v \sim 0$ km s^{-1}
log N(Zn II)	12.43	12.88
log N(Fe II)	15.27	14.97
log N(Si II)	15.50	15.96
log N(S II)	15.16	15.55
[Zn/Fe]	0.00	+0.75
[S/Si]	0.01	−0.06
[S/Zn]	0.18	0.12

6.1 Aluminium

A natural probe of the level of ionization in a DLA is to compare column densities of different ionization states of a given element. The relative column densities depend on the ionization potentials, the shape of the ionizing spectrum and the density of the gas (or, equivalently, the ionization parameter). The ratio of Al III/Al II is sometimes used as a crude estimate of ionization, although Si II is often substituted for Al II which saturates quickly. Vladilo et al. (2001) showed a broad anti-correlation of Al III/Al II with N(H I) supporting the idea that this ratio traces the amount of ionized gas. In Fig. 12 we show Al III/Al II and Al III/Si II for our PDLA and comparison DLA sample, where the latter ratio is corrected for the solar value of (Si/Al). There is no obvious difference between the DLA and PDLA ratios, certainly there is no indication of elevated amounts of Al III at a given N(H I) in PDLAs relative to DLAs. In fact, several PDLAs appear to have fairly low Al III/Si II. However, as discussed by Howk & Sembach (1999) Al III may actually be a fairly poor tracer of ionized gas in intervening absorbers and may even originate from a different region in the absorber (Vladilo et al. 2001). Moreover, the behaviour of Al III/Al II is very sensitive to the shape of the ionizing spectrum. Vladilo et al. (2001) use CLOUDY photoionization models to demonstrate that for a hard (QSO) ionizing spectrum the observed Al III/Al II is essentially flat as a function of N(H I), for a given ionization parameter (log U). Therefore, whilst adopting a stellar ionizing spectrum seems to naturally reproduce the trend of decreasing Al III/Al II with increasing N(H I) for a given ionization parameter, assuming a hard spectrum requires the log U to decrease at higher N(H I) to produce the same anti-correlation (see also Vladilo et al. 2003). It requires a very intense power-law spectrum ($\log U \gtrsim -1$) in order to achieve N(Al III) > N(Al II), so the relatively low ratios of Al III/Si II observed in Fig. 12 do not rule out proximity to a hard ionizing source. In fact, a hard ionizing spectrum may actually be the reason for the lower Al III/Si II ratios at log N(H I) < 21 in the PDLAs compared to intervening DLAs. The stellar ionizing models of Vladilo et al. (2001) generally predict higher Al III/Al II at low N(H I) for soft spectra relative to QSO-like radiation.

6.2 Silicon

Next, we consider the relative abundances of Si II and Si IV. Si II is detected in all seven PDLAs in our sample. There are four Si IV

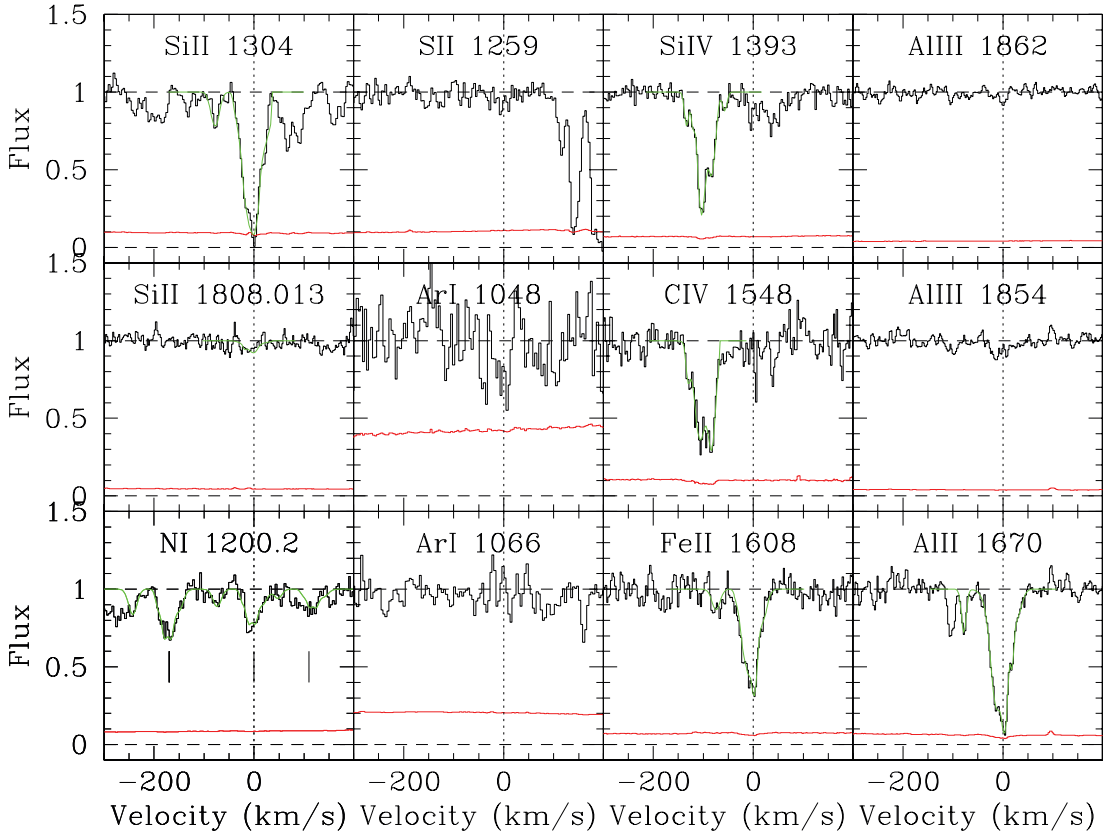

Figure 11. Selected metal line transitions in the PDLA towards J2321+1421. The lower solid (red) line shows the error array. When fits have been derived using VPFIT, those fits are overlaid in green. *b*-values for this absorber range from 2 to 12 km s^{-1} for the low ionization species and 5 to 25 km s^{-1} for the higher ionization species. Velocities are plotted relative to $z_{\rm abs} = 2.5731$. The vertical ticks in the lower left panel show the strongest components in each of the N I triplet lines.

Table 7. Candidate PDLAs taken from the literature. Redshifts without error bars are taken from Prochaska et al. (2008b). The final column indicates whether the absorber is included in our PDLA sample, which requires that $\Delta V < 3000\,{\rm km\,s^{-1}}$.

QSO	$z_{\rm em}$ lit.	$z_{\rm abs}$	ΔV lit. (km s^{-1})	$z_{\rm em}$ new	ΔV new (km s^{-1})	Include?
Q1157+014	1.990	1.944	4651	1.9920 ± 0.003	4851	N
J2340−00	2.090	2.054	3516	2.0829 ± 0.003	2825	Y
Q2222−3939	2.18	2.154	2463	2.1832 ± 0.007	2765	Y
Q0425−5214	2.25	2.224	2410	2.2639 ± 0.007	3690	N
Q0841+12	2.500	2.476	2064	2.4934 ± 0.003	1498	Y
B0405−331	2.570	2.569	84	2.5775 ± 0.006	714	Y
Q2343−BX415	2.57393	2.5720	162	2.5742 ± 0.0005	22	Y
Q0528−2505	2.779	2.812	−2608	2.7783 ± 0.007	−2664	Y
Q1354−1046	3.007	2.967	3010	3.0112 ± 0.010	3324	N
Q2059−360	3.09	3.083	514	3.0974 ± 0.009	1056	Y
SDSS2100−0641	3.140	3.0924	3469	3.1295	2707	Y
J0900+42	3.290	3.2458	3107	3.2954	3484	N
J0255+00	3.988	3.915	4423	3.9936	4759	N
PSSJ0957+33	4.227	4.178	2826	4.2088	1779	Y

detections, two lower limits (from saturated lines) and one upper limit from a non-detection. For the two PDLAs with log N(H I) < 20.4 (Q0151+048 and J0142+0023), we find that log[N(Si IV)/N(Si II)] = −0.26 and −0.42, respectively. Such high fractions of Si IV are relatively rare in intervening DLAs. The other PDLAs where Si IV has a detection or upper limit have Si IV/Si II fractions less than 10 per cent. In cases where intervening DLAs exhibit Si IV, it is usually observed in a different velocity structure from Si II (Wolfe & Prochaska 2000), which can be obtained if the ionizing spectrum is relatively soft (Howk & Sembach 1999). This is indeed the case for the PDLAs towards J2321+1421 and J0142+0023 where the bulk of the Si IV is offset from the Si II. However, for 3/6 of the PDLAs in our sample where we detect Si IV, it traces the structure of the Si II (Q0151+048, J1131+6044, J1604+3951). This is unusual; one explanation could be the presence of a hard spectrum (and/or high ionization parameter). For the final PDLA where Si IV is detected (J1240+1455) the Si IV is so strongly saturated

Table 8. Column densities (in cm^{-2}) for final literature PDLA sample. References: 1: Akerman et al. (2005); 2: Lu et al. (1996); 3: Centurión et al. (2003); 4: Noterdaeme et al. (2008); 5: P. Noterdaeme private communication; 6: Dessauges-Zavadsky et al. (2007); 7: Srianand et al. (2005); 8: Herbert-Fort et al. (2006); 9: Prochaska et al. (2001); 10: Prochaska et al. (2003b); 11: Rix et al. (2007); 12: Prochaska et al. (2007b); 13: this work.

QSO	z_{abs}	log N(H I)	log N(Fe II)	log N(Zn II)	log N(Si II)	log N(Cr II)	log N(S II)	[Si/H]	Reference
J2340−00	2.054	20.35 ± 0.15	>14.97	12.63 ± 0.08	15.17 ± 0.04	<12.90	14.94 ± 0.05	−0.69	12,13
Q2222−3939	2.154	20.85 ± 0.10	14.42 ± 0.03	<11.70	14.55 ± 0.05	12.77 ± 0.04	14.08 ± 0.02	−1.81	4,5
Q0841+12	2.476	20.78 ± 0.08	14.50 ± 0.03	11.69 ± 0.10	14.99 ± 0.03	12.89 ± 0.06	14.48 ± 0.10	−1.30	6
B0405−331	2.569	20.60 ± 0.10	14.33	<12.74	14.74	<13.32	–	−1.37	1
Q2343−BX415	2.5720	20.98 ± 0.05	15.24 ± 0.02	12.90 ± 0.06	15.79 ± 0.04	13.58 ± 0.04	15.38 ± 0.03	−0.70	11
Q0528−2505	2.812	21.11 ± 0.04	15.47 ± 0.02	13.27 ± 0.03	16.01 ± 0.03	13.65 ± 0.12	15.56 ± 0.02	−0.61	2,3
Q2059−360	3.083	20.98 ± 0.08	14.52 ± 0.07	–	14.80 ± 0.05	–	14.41 ± 0.04	−1.69	7
SDSS2100−0641	3.0924	21.05 ± 0.15	15.36 ± 0.03	<13.14	15.89 ± 0.02	13.69 ± 0.04	15.52 ± 0.01	−0.67	8
PSSJ0957+33	4.178	20.65 ± 0.15	14.13 ± 0.05	–	14.56 ± 0.01	–	14.39 ± 0.06	−1.60	9,10

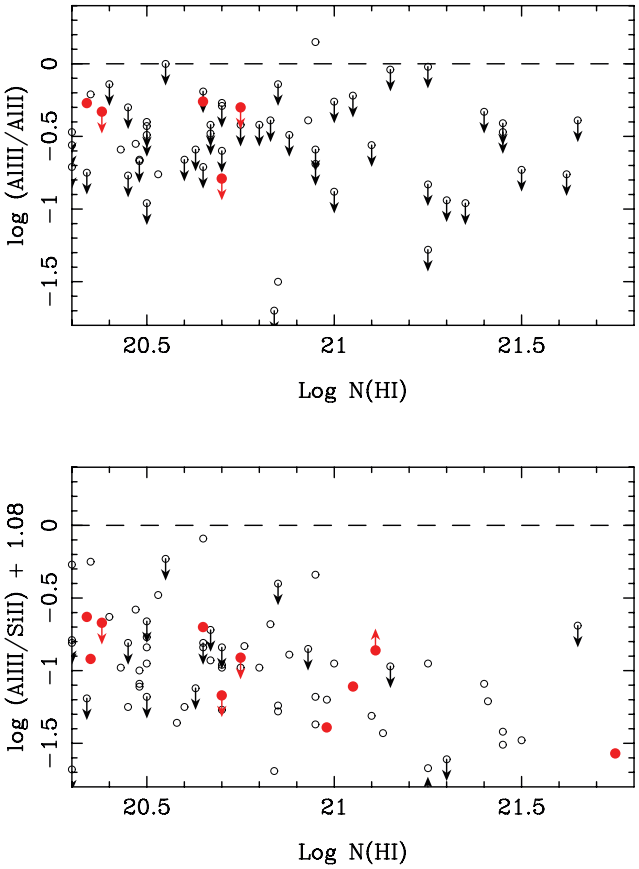

Figure 12. Al III/Al II (top) and Al III/Si II (bottom) as a function of N(H I) for intervening DLAs (open points, $\Delta V > 10\,000$ km s^{-1}) and PDLAs (filled points, $\Delta V < 3000$ km s^{-1}).

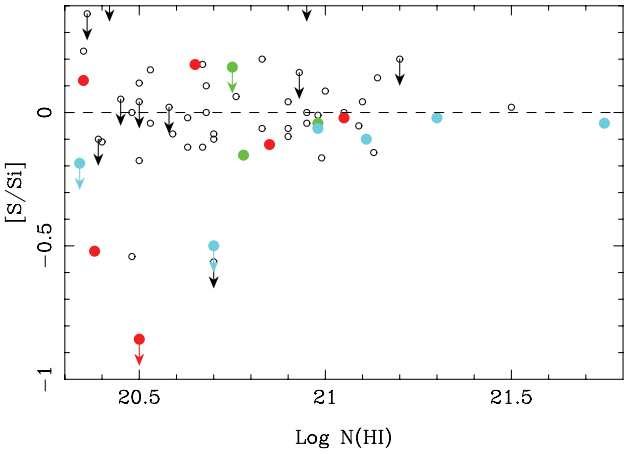

Figure 13. [S/Si] as a function of log N(H I) for intervening DLAs (open points, $\Delta V > 10\,000$ km s^{-1}) and PDLAs (filled coloured points) from the new data presented here and taken from the literature (see Table 8). PDLAs are colour coded by their relative velocities (see Table 2): cyan for $\Delta V < 500$ km s^{-1}, green for $500 < \Delta V < 1500$ km s^{-1} and red for $\Delta V > 1500$ km s^{-1}. The low values of [S/Si] cannot be easily explained by dust depletion or nucleosynthesis and may be caused by ionization by a hard radiation source.

we have no information on its velocity structure. Interestingly, the coincident (or not) velocity structure of Si IV with Si II is independent of the ΔV of the PDLA. For example, J2321+1421 has the smallest velocity separation (−1616 km s^{-1}) with little or no Si IV coinciding with Si II, yet the largest ΔV PDLA (J1131+6044, 2424 km s^{-1}) has very similar velocity structure in the two ions.

6.3 Alpha elements

S, Si, Ar and O are all α capture elements that are produced predominantly in massive stars. Their shared nucleosynthetic origin leads to approximately solar abundance ratios of these elements in Galactic stars (e.g. Chen et al. 2002). Departures from solar ratios in DLAs can occur when one or both of the α elements in question are depleted from the gas phase on to dust, or if there is significant ionization. O I is an ideal 'anchor' to study α elements since oxygen is both relatively undepleted (Savage & Sembach 1991) and O I requires a negligible ionization correction. Unfortunately, the most accessible O I transition ($\lambda_0 = 1302$ Å) is usually strongly saturated. We have only one PDLA in our sample with a well-constrained column density of O I; the other absorbers yield only lower limits.

We have detections or meaningful limits for S and Si for all the PDLAs in our sample. Like O, S is largely undepleted in the Galactic ISM, but Si is mildly refractory. Super-solar ratios of [S/Si] may therefore be observed if dust is present. In Fig. 13 we plot [S/Si] versus N(H I) for the sample of seven new PDLAs plus systems taken from the literature (see Table 8). PDLAs are colour-coded by their relative velocity, and intervening DLAs with $\Delta V > 10\,000$ km s^{-1} are shown for comparison as open circles. The intervening DLAs cluster around [S/Si] = 0 with most points within ±0.2 dex of the solar ratio. The effects of dust depletion appear to be relatively mild (i.e. few DLAs show highly super-solar [S/Si]). The PDLAs also cluster around the solar ratio, but only when log N(H I) ≥ 20.75. At least 50 per cent (accounting for limits) of the lower N(H I)

PDLAs have [S/Si] that is several tenths of a dex below that of the intervening systems. Since neither nucleosynthesis nor depletion is expected to lower the [S/Si], the deviation from the solar ratio may be due to ionization effects. This hypothesis is supported by the tendency of low [S/Si] ratios to be observed only at lower N(H I) PDLAs. Photoionization modelling indeed indicates that S and Si require corrections of opposite sign in the presence of a power-law spectrum (Rix et al. 2007). Interestingly, the trend of low [S/Si] at low N(H I) does not seem to depend solely on ΔV. Even at $\Delta V > 1500$ km s^{-1}, 2/3 PDLAs with log N(H I) ≤ 20.5 show very sub-solar [S/Si] ratios. Conversely, PDLAs with very small velocity separations exhibit solar [S/Si] when log N(H I) > 21, indicating that they are well-shielded despite a small velocity separation. However, we caution that many of the relative velocities are constrained only to within $\pm$500 km s^{-1} and that ΔV is not necessarily an indication of physical proximity.

A natural concern in the interpretation of Fig. 13 is that it relies on several limits in PDLAs resulting from the non-detection of S II. As discussed in Section 4, the calculated limit is somewhat sensitive to the assumed width of the line. In order to check our calculated S II detection limits we produced Voigt profiles of S II λ 1259 for the limiting column density, adopting the b-value and redshift of the strongest component in the fit to one of the low ions (either Si II or Fe II). A visual inspection of the calculated limits overlaid on the data indicates that they are reasonable estimates.

Argon is relatively rarely measured in DLAs, mostly due to frequent blending of the rest-frame far-UV lines of Ar I at $\lambda =$ 1048, 1066 Å. However, the abundance of Ar I is very sensitive to ionization, because its ratio of photoionization to recombination rates is typically one order of magnitude higher than for H I (Sofia & Jenkins 1998). Interestingly for our study, Vladilo et al. (2003) have used CLOUDY modelling to demonstrate that the fraction of Ar I is sensitive to the adopted radiation field. Low ratios of Ar relative to other alpha elements are expected when the radiation field is hard, whereas the models predict solar ratios when the ionizing spectrum is soft. Two of our limits on [Ar/Si] are not deep enough to be very meaningful: [Ar/Si] $< +0.42$, -0.01 towards J0140−0839 and J2321+1421, respectively. The two other limits are very sub-solar: [Ar/Si] < -0.86, -0.47 towards J1131−6044 and J0142+0023, respectively. We have one new argon detection (towards J1604+3951), although we can only derive its ratio with silicon for the principal component: [Ar/Si] $= -0.40$. Sub-solar ratios of [Ar/Si] are therefore apparently common in the PDLAs and further support significant ionization by a hard radiation field.

6.4 Nitrogen

The most highly ionized species available for the study in our sample is N V (in all cases O VI is blended). Fox et al. (2009) find a 13^{+5}_{-4} per cent N V detection rate in DLAs compared with 13^{+18}_{-9} per cent in PDLAs out to 5000 km s^{-1} from the QSO. This result may seem surprising given the ionization radiation from the nearby QSO. Indeed, Fechner & Richter (2009) find a high N V incidence rate amongst $\Delta V < 5000$ km s^{-1} absorbers with $13 <$ log N(H I) $<$ 17.0. Fox et al. (2009) suggest that the consistency in N V detection rates between DLAs and PDLAs may be due to the fairly large velocity interval over which they include a DLA in their proximate sample. In our sample, 2/7 (J1240+1455 and J1604+3951) of the PDLAs exhibit N V at a similar velocity to the low ions – tentative evidence that N V is more common in PDLAs, although better statistics are required to confirm this. Notably, the PDLA towards J1240+1455 exhibits one of the largest N(N V) yet reported in the literature (Fox et al. 2009). The two N V detections in our sample occur in PDLAs with small ΔV, high N(H I) and relatively high metallicity ($Z \sim 1/10\,Z_\odot$). Rix et al. (2007) also detected N V in the N(H I) = 20.98 PDLA towards Q2343−BX415, which also has a fairly low velocity separation ($\Delta V = 22$ km s^{-1}) and high metallicity ($Z \sim 1/5\,Z_\odot$). However, J2321+1421 which has the largest negative velocity in our sample (~ -1600 km s^{-1}) does not exhibit N V. The detection rate of N V would therefore increase if we limited our statistics to lower ΔV, supporting the explanation of Fox et al. for the lack of N V excess in their proximate sample. The higher incidence of N V out to 5000 km s^{-1} seen by Fechner & Richter (2009) may be associated with the lower N(H I) column densities of their sample.

7 ABUNDANCES

7.1 Metallicity

Fig. 14 shows Fe and Si abundances as a function of redshift for DLAs and PDLAs whose redshifts are $z_{\rm abs} > 1.8$. Our sample includes PDLAs that are amongst both the most metal-poor and the most metal-rich for their redshift. The PDLA towards J0140−0839 has the lowest metallicity ever detected in a high N(H I) absorber (see Section 4.1 for further discussion), although there may be an

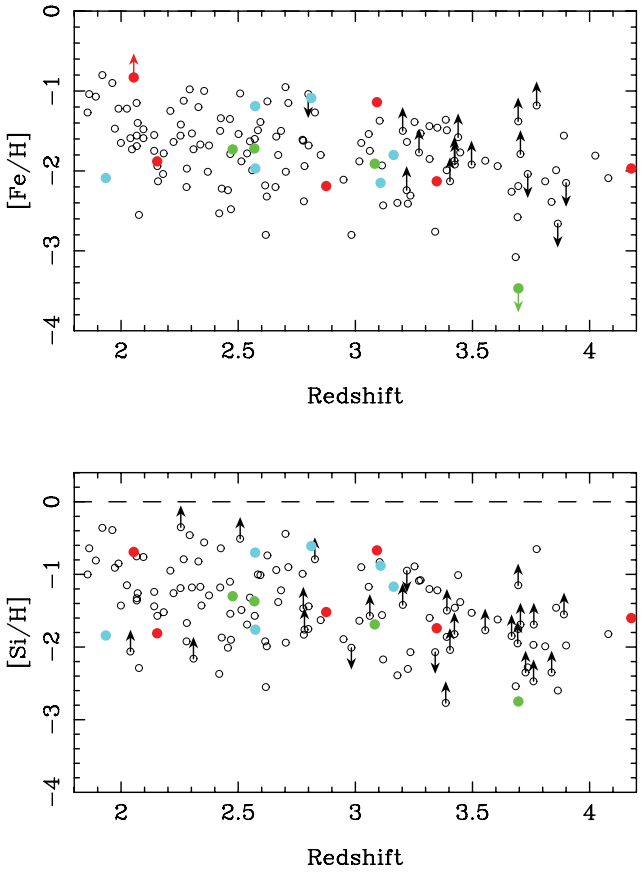

Figure 14. Si and Fe abundances as a function of absorption redshift for intervening DLAs (open points, $\Delta V > 10\,000$ km s^{-1}) and PDLAs (filled coloured points). PDLAs are colour coded by their relative velocities (see Table 8): cyan for $\Delta V < 500$ km s^{-1}, green for $500 < \Delta V < 1500$ km s^{-1} and red for $\Delta V > 1500$ km s^{-1}. There is a large scatter in both Si and Fe abundances in PDLAs at a given redshift (see Section 7.1).

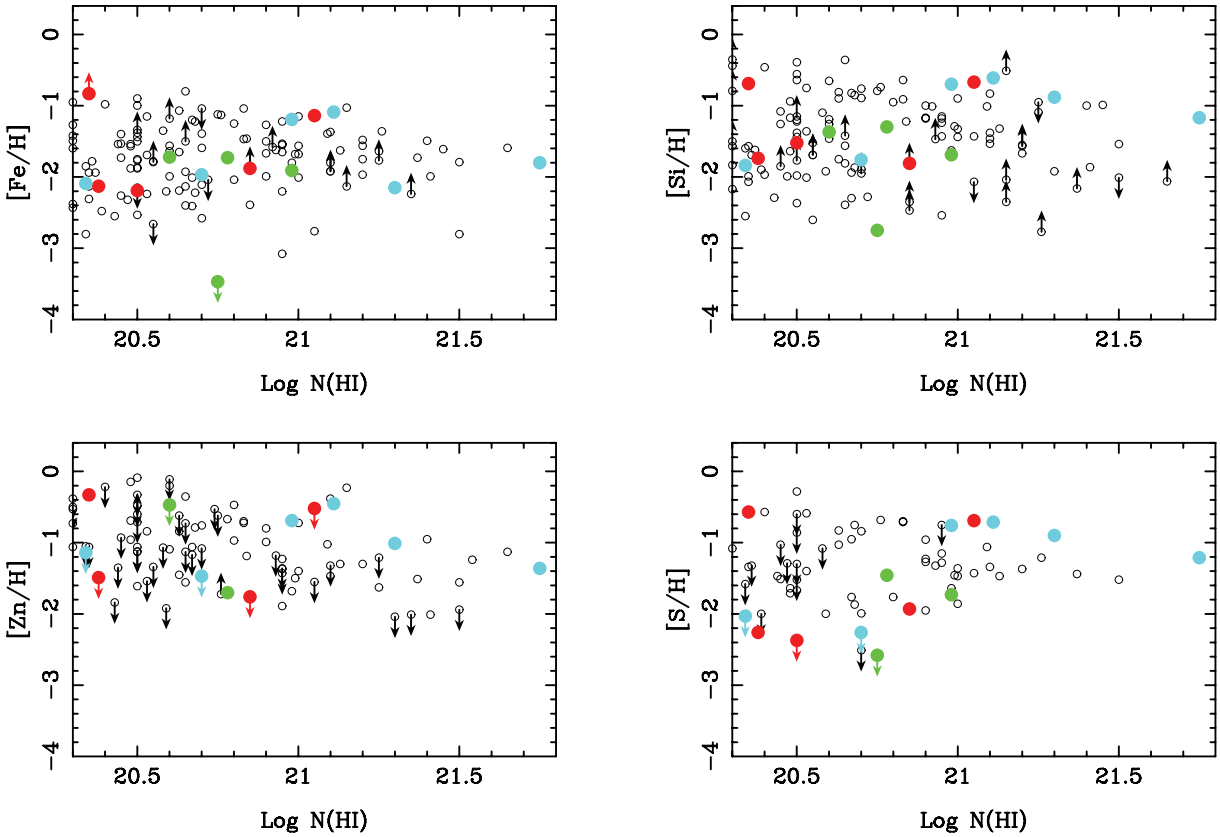

Figure 15. Si, Fe, Zn and S abundances as a function of log N(H I) for intervening DLAs (open points, $\Delta V > 10\,000$ km s^{-1}) and PDLAs (filled coloured points). Si and Fe are either mildly or severely depleted by dust, whereas Zn and S are largely undepleted from the gas phase and may therefore represent more reliable indicators of metallicity. PDLAs are colour coded by their relative velocities (see Table 8): cyan for $\Delta V < 500$ km s^{-1}, green for $500 < \Delta V < 1500$ km s^{-1} and red for $\Delta V > 1500$ km s^{-1}. Silicon and sulphur (and to a lesser extent zinc) exhibit high abundances when log N(H I) > 21 (see Section 7.1).

upwards correction of up to a few tenths of a dex to be made for ionization. The results in Fig. 14 ostensibly support the conclusion of Rix et al. (2007) that PDLAs exhibit metallicities that span the distribution of intervening DLAs. However, in Section 6 it is argued that the low N(H I) systems are likely to have significant ionization corrections. We therefore re-assess the PDLA metallicities as a function of N(H I).

PDLAs with log N(H I) > 21 probably have negligible ionization corrections and Fig. 15 shows that these PDLAs have quite high [Si, S/H]. The Zn abundances are also distributed towards the upper end of the intervening DLA distribution. [Fe/H] shows more scatter and its sensitivity to dust depletion makes it harder to interpret. At lower N(H I), all but one of the PDLAs have Si and S abundances that are below the median. This intriguing observation could be interpreted as a difference in the provenance of the low and high N(H I) PDLAs. Alternatively (and perhaps more likely) it could indicate that the PDLAs (or at least a subset thereof) have intrinsically higher metallicities, but whose abundance determinations are affected by ionization at low N(H I).

7.2 Dust depletion indicators

In Fig. 16, we plot the [Zn/Fe] ratio (as an indicator of depletion) as a function of [Zn/H] for the PDLA and DLA samples. The median [Zn/Fe] for our literature sample (when both Zn and Fe are measured) is [Zn/Fe] $\sim +0.4$. J1240+1455 appears to have particularly high depletion, although at $Z \sim 1/10\,Z_{\odot}$ it is also one

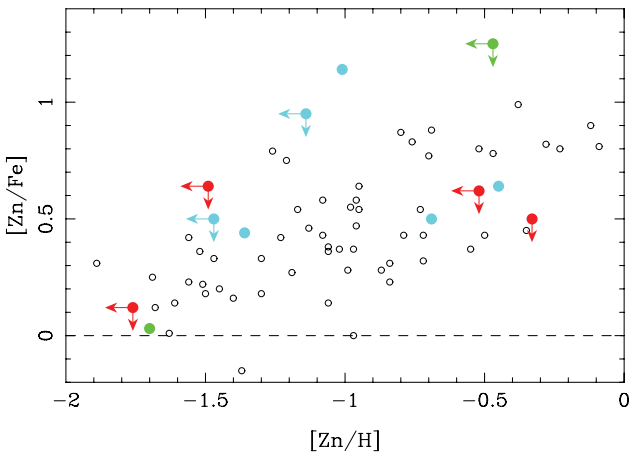

Figure 16. [Zn/Fe] as a function of [Zn/H] for intervening DLAs (open points, $\Delta V > 10\,000$ km s^{-1}, limits excluded for clarity) and PDLAs (filled coloured points). PDLAs are colour coded by their relative velocities (see Table 8): cyan for $\Delta V < 500$ km s^{-1}, green for $500 < \Delta V < 1500$ km s^{-1} and red for $\Delta V > 1500$ km s^{-1}. The PDLAs show no distinct dust depletion trends compared with the intervening absorbers (see Section 7.2).

of the more metal-rich absorbers. The PDLA towards J1240+1455 has a high N(H I) so the high [Zn/Fe] ratio is unlikely to be caused by ionization. J1604+3951 shows clear signs of different levels of depletion between two velocity components with high [Zn/Fe] in

one component but not the other (see Section 4.6). Overall, there is no obvious difference between the dust depletion in the PDLAs and the intervening systems.

7.3 Alpha elements

[Si/Fe] is used as an indicator of α enhancement, since both elements are measured in the majority of our sample. [Si/Fe] is usually plotted as a function of metallicity, although the results presented so far in this paper indicate that trends may also be present with N(H I) due to ionization. In Fig. 17 we therefore plot [Si/Fe] as a function of both N(H I) and [Si/H]. Fig. 17 shows that at low N(H I) the PDLAs have fairly typical values of [Si/Fe], with the exception of the very metal poor PDLA towards J0140−0839 which has [Si/Fe] ≥ 0.72. This PDLA is even more of an outlier when its [Si/Fe] is considered relative to its metallicity. Although the high [Si/Fe] ratio could be due in part to ionization corrections and/or dust, it also raises the intriguing possibility of extreme α element enhancement in a chemically young object. SDSS offers the opportunity to search out other rare, low metallicity DLAs in order to investigate their nucleosynthetic histories. The [O/Fe] ratio in this absorber is also high, [O/Fe] ≥ 0.75 and O I is much less affected by ionization and dust than Si II. J1131+6044 also has a relatively high value of [Si/Fe] $= 0.67$, although Fig. 17 shows that such values are not unknown in the intervening population. J1240+1455 has an extremely high [Si/Fe] that is unlikely to be due to ionization effects, given its high N(H I). However, as discussed in the previous section, the [Zn/Fe] indicates a large depletion fraction which could lead to an overestimate of [Si/Fe] (Fe is much more refractory than Si). Using the undepleted ratio of [S/Zn] $= 0.11$, the high [Si/Fe] of J1240+1455 appears to be largely due to dust. In summary, there are no clear, systematic differences in the [Si/Fe] ratios of PDLAs compared with the intervening systems, although some PDLAs do appear to have relatively high values.

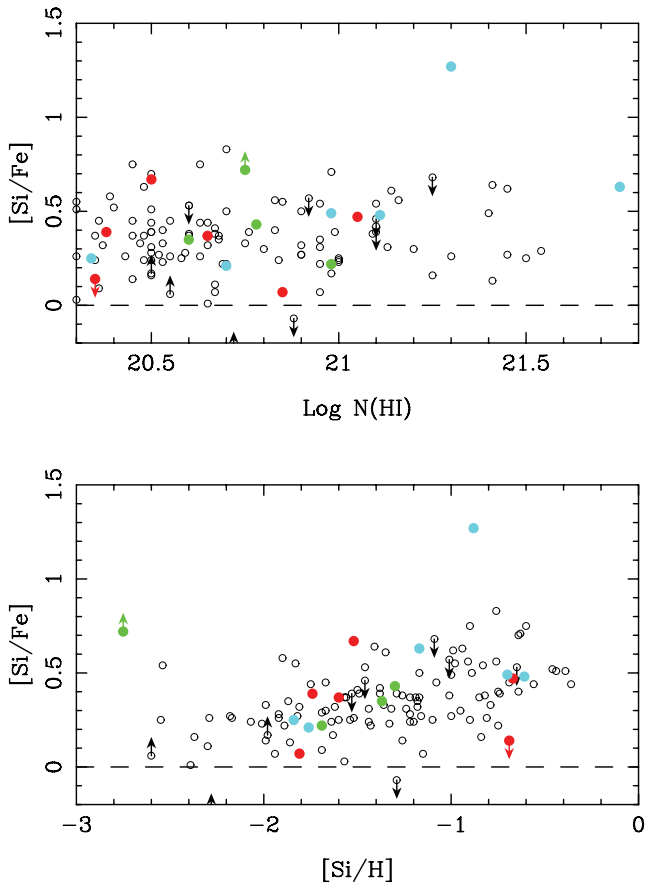

Figure 17. [Si/Fe] as a function of [Si/H] (bottom panel) and log N(H I) (top panel) for intervening DLAs (open points, $\Delta V > 10\,000$ km s^{-1}) and PDLAs (filled coloured points). PDLAs are colour coded by their relative velocities (see Table 8): cyan for $\Delta V < 500$ km s^{-1}, green for $500 < \Delta V < 1500$ km s^{-1} and red for $\Delta V > 1500$ km s^{-1}. The PDLAs show no distinct [α/Fe] trends compared with the intervening absorbers (see Section 7.3).

8 CONSTRAINING THE DISTANCES TO PDLAS FROM FINE-STRUCTURE LINES

We have emphasized in this paper that the velocity offsets (ΔV) between the QSO and PDLAs are unlikely to be convertible into distances using Hubble's law. To attempt to constrain the true physical distances we can model the interplay between the QSO's radiation and the PDLA's interstellar gas.

8.1 Distances from C II*

In this section we describe the method for using C II* to estimate the PDLA–QSO distance, as well as describing the assumptions of the model, limitations and caveats. The practical application of the method is given in Section 8.1.1.

Wolfe, Prochaska & Gawiser (2003) have used C II* to estimate the radiation intensity, and hence the star formation rate in DLAs. The far UV radiation emitted by massive stars contributes to heating through the grain photoelectric effect, which in turn heats the gas. The heating rate, Γ, is a function of the mean radiation intensity (J), the heating efficiency (ϵ) and the dust-to-gas ratio relative to the Galactic value (κ): $\Gamma \propto J\epsilon\kappa$. The value of ϵ is known from Galactic studies (e.g. Bakes & Tielens 1994), and κ can be inferred from ratios of refractory to undepleted elements for individual DLAs, under an assumed model for dust depletion patterns and intrinsic abundance ratios. In a plane-parallel layer J is proportional to $\psi_\star$, the star formation rate per unit area (which we henceforth refer to as simply 'star formation rate' for brevity). The star formation rate can therefore be determined once Γ is known. This is achieved by assuming that the medium is in local thermal equilibrium and that heating rate can thus be equated to the cooling rate. This latter quantity is inferred from the C II* absorption line which measures the population of the excited $^2P_{3/2}$ fine-structure state that spontaneously decays to the ground-state by emitting a 158 μm photon.

For PDLAs, a second source of far UV photons potentially contributes to the heating: radiation directly from the proximate QSO. Rix et al. (2007) measured C II* in one PDLA and by assuming that all the radiation originated from the QSO placed a lower limit on the distance of the PDLA from the QSO. We follow a similar procedure here, but calculate the distance as a function of $\psi_\star$ to explore the range of likely values of the PDLA–QSO separation. We assume that the mean radiation intensity, J, inferred from C II* has contributions from star formation and the QSO:

$$J_{\rm TOT} = J_{\rm SF} + J_{\rm QSO}. \quad (5)$$

The radiation contribution from the QSO depends on the QSO luminosity (L_ν) and separation (d). J is measured in erg cm^{-2} s^{-1} sr^{-1} Hz^{-1} so that

$$4\pi J_{{\rm QSO},\nu} = \frac{L_\nu}{4\pi d^2}. \quad (6)$$

The C II* analysis of Wolfe et al. (2003) yields J for a rest wavelength of 1500 Å.

Table 9. PDLA–QSO distance calculations. Solutions are given for the C II* analysis under the assumption of a CNM and for Si II* where suitable detections/limits are possible (see text for details).

QSO	$z_{\rm abs}$	ΔV (km s^{-1})	log N(C II*) (cm^{-2})	log N(Si II*) (cm^{-2})	L_{1500} (erg s^{-1} Hz^{-1})	$d_{\rm CNM}$ (kpc) $\psi_\star = 0$	$d_{\rm CNM}$ (kpc) log $\psi_\star = -2.4$	$d_{\rm Si\,II^\star}$ (kpc)
J0140−0839	3.6960	1250	<12.41	<11.48	1.08×10^{32}	>2099.0	–	>14.8
J0142+0023	3.34765	1772	–	<11.17	4.76×10^{31}	–	–	>29.8
Q0151+048	1.9342	−1199	13.0	< 11.81	2.44×10^{31}	160.5	406.0	>8.6
J1131+6044	2.8754	2424	<12.51	<11.57	5.85×10^{31}	–	–	>30.8
Q2321+1421	2.5731	−1616	<12.55	<11.78	2.27×10^{31}	>510.1	–	>14.3

Combining equations (5) and (6) and solving for d, we obtain

$$d = \frac{1}{4\pi}\sqrt{\frac{L_\nu}{J_{{\rm TOT},\nu} - J_{{\rm SF},\nu}}}. \quad (7)$$

The contribution to J from star formation depends on the geometry of the plane-parallel layer (parametrized by the ratio of its radius and height, R/h), metallicity and its dust-to-gas ratio, k_ν. For $k_\nu h \ll k_\nu R \ll 1$ equations (18) and (19) of Wolfe et al. (2003) can be reduced and re-arranged to give

$$J_{{\rm SF},\nu} = 8.4 \times 10^{-16}\psi_\star . \frac{1 + \ln(R/h)}{8\pi} \quad (8)$$

where $\psi_\star$ is measured in units of M$_\odot$ yr^{-1} kpc^{-2}. A fixed aspect ratio of $R/h = 20$ is used for all calculations. Following Wolfe et al. (2003), the dust-to-gas ratio is determined from Si/Fe and metallicity from [Si/H] with an assumed intrinsic [Si/Fe] = 0.2 and SMC depletion patterns. Solutions can be calculated for two cases: gas that is dominated by the cold and warm neutral media (CNM, WNM), respectively. However, using C II* to constrain distances for the WNM solutions has two problems. First, in the WNM, the cooling is actually dominated not by the [C II] 158 μm transition, but by Lyα and the recombination of electrons on to grains. Second, at the low densities implied by the WNM solutions, the dominant heating source is no longer the grain photoelectric effect, but cosmic ray heating and, to a lesser extent, heating by X-rays. In the calculations of Wolfe et al. (2003), the cosmic ray production rate is assumed to scale with the star formation rate. However, we are additionally concerned with energy sources associated with the QSO and it is unclear whether active galactic nuclei (AGN) produce cosmic rays and at what rate. We therefore only consider the CNM solutions, but caution that these are probably inappropriate for the PDLAs with the lowest cooling rates. A full treatment of the WNM solutions for AGN heating is beyond the scope of this paper.

The QSO luminosity at $\lambda_0 = 1500$ Å is determined from the SDSS spectrum, except in the case of Q0151+048. For this target, we take $B_{\rm AB} = 17.83$ from Fynbo et al. (2000) which converts to a flux of 2.7×10^{-27}erg s^{-1} Hz^{-1} (no corrections are made for Lyα emission or Lyα forest absorption, since they lie outside the B filter for $z = 1.9$). The luminosity and flux (in units of erg s^{-1} Hz^{-1}) at a given frequency are related through the equation

$$F_\nu = L_{(1+z)\nu} \times \frac{1+z}{4\pi d_{\rm L}^2} \quad (9)$$

where $d_{\rm L}$ is the luminosity distance in our adopted cosmology. In Table 9, we list the calculated values of L_{1500}.

In the previous sections, we have argued that ionization may lead to errors in the column densities that we measure, particularly at low N(H I). The metallicity (nominally [Si/H]) and dust-to-gas ratio (calculated from [Si/Fe]) are required to calculate $J_{\rm TOT}$. However, Wolfe et al. (2003) have shown that $J_{\rm TOT}$ is actually relatively insensitive to the metallicity used for values $Z \lesssim 1/10\,{\rm Z}_\odot$. Even at the highest metallicities, incorrect values of [Si/H] are likely to affect $J_{\rm TOT}$ by less than 20 per cent. Uncertainties in the dust-to-gas ratio are potentially more problematic, since the grain photoelectric effect can be a dominant source of ISM heating. However, the contribution of this process to the heating budget depends on the ISM density (e.g. fig. 3 in Wolfe et al. 2003), becoming more dominant at high densities. For CNM solutions, lower dust-to-gas ratios (i.e. fewer grain targets for heating) require a higher incident intensity to account for the observed C II*.[7] However, in Section 7.3 we showed that the range of [Si/Fe] ratios of most of the PDLAs are in good agreement with intervening systems. Assuming that there is an intrinsic 'floor' to [Si/Fe] whose value is approximately 0.2 (e.g. Prochaska & Wolfe 2002) and given that ionization effects tend to lead to overestimates of [Si/Fe] (e.g. Dessauges-Zavadsky et al. 2003; Howk & Sembach 1999), the measured Si/Fe ratios do not indicate significant corrections in the majority of cases.

8.1.1 Application to the data

C II* is detected in Q0151+048 and J1604+3951 and we have upper limits for J0140−0839, J1131+6044 and J2321+1421 which will yield lower distance limits for a given $\psi_\star$. However, the C II* towards J1604+3951 is partly blended with C II λ 1334, and the unblended components are saturated, so we do not consider this PDLA further. Q0151+048 may have $J_{\rm QSO}$ contributions from Q0151+048B, introducing a second unknown distance. Fynbo et al. (1999) have argued that the most likely orientation of the system is that Q0151+048B is in front of Q0151+048 and the DLA and causes Lyα emission on the near face of the absorber. Modelling this system completely is complicated not just by uncertainty in the geometry of the QSO pair and absorber, but also by the anisotropy of quasar radiation and hence the flux 'seen' by the DLA coming from Q0151+048B. However, assuming that all the flux comes from the background QSO still yields a lower limit to the distance between Q0151+048 and the PDLA (just as we determine a lower limit under the assumption that internal star formation does not contribute).

In Table 9, we list the limiting value of the PDLA–QSO distance for a star formation rate $\psi_\star = 0$ and also the fiducial case of a Galactic star formation rate of log $\psi_\star = -2.4\,{\rm M}_\odot\,{\rm yr}^{-1}\,{\rm kpc}^{-2}$ for the CNM solutions. For PDLAs with upper limits to N(C II*) the CNM solutions are likely to be inappropriate and they are given in the table only for completeness. More sensitive C II* limits could definitively rule out CNM solutions entirely as is the case for J1131+6044 which only has a WNM solution. The C II* analysis therefore only yields a useful distance constraint for Q0151+048 where the lower

[7] As discussed in the text, at low densities cosmic ray heating dominates over the grain photoelectric effect. WNM solutions, although not pursued here, are therefore very insensitive to the input value of [Si/Fe].

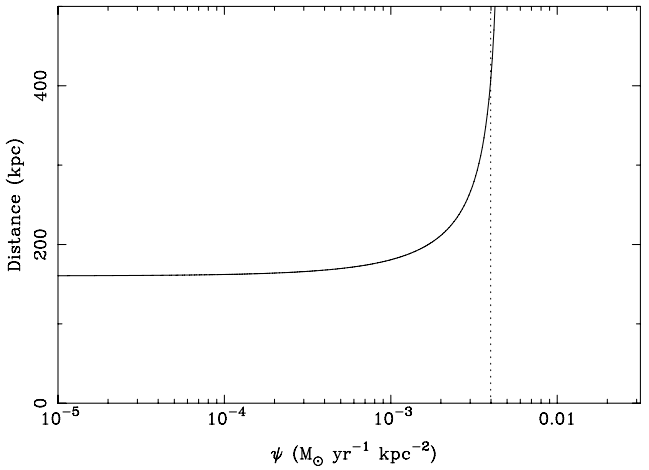

Figure 18. Distances between the PDLA and Q0151+048 calculated from the C II* analysis. The curve shows the distance corresponding to an increasing local contribution of radiation from star formation rate, log $\psi_\star$. The vertical dotted line indicates log $\psi_\star = -2.4\,M_\odot$ yr^{-1} kpc^{-2}.

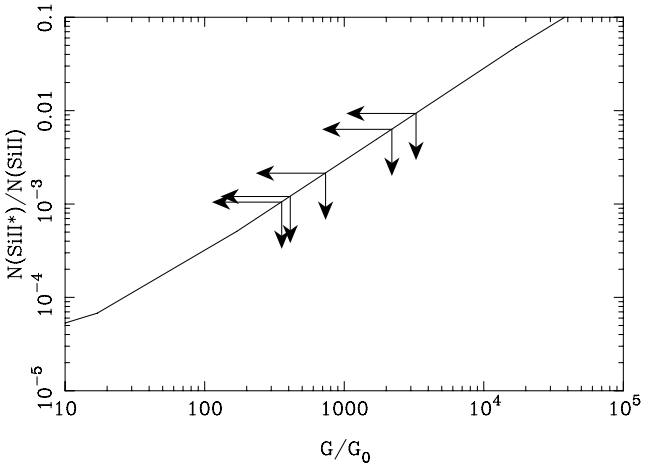

Figure 19. Ratio of fine structure to ground state column densities from UV pumping determined from the POPRATIO software. The arrows indicate the inferred upper limit of the incident radiation field in units of the Galactic value based on upper limits of N(Si II*).

limit is 160 kpc (no star formation case), rising to just over 400 kpc for a Galactic star formation rate, a separation approximately five times larger than the only other PDLA in the literature has been analysed in this way (Q2343−BX415 by Rix et al. 2007). In Fig. 18 we show the complete range PDLA–QSO distances as a function of star formation rate for Q0151+048. The figure demonstrates that once star formation dominates over the QSO's radiation, the inferred distance to the PDLA rises dramatically, essentially providing an upper limit to the likely star formation rate in the galaxy, as well limits of the distance to the QSO.

8.2 Distance constraints from Si II* limits

There are a number of uncertainties and assumptions that underpin the distance calculations from C II* which affect the inferred radiation field to varying extents. These include the knowledge of the gas phase (cold or warm), metallicity, dust depletion, assumed geometry and extinction law. An alternative assessment of the distance between the absorber and the radiation source can be made using the Si II fine-structure lines and the ratio of N(Si II*) to the column of the ground state ions. In order to determine the relation between N(Si II*)/N(Si II) and the incident radiation field, we use the publicly available code POPRATIO (Silva & Viegas 2002). We assume that Si II* is populated purely by UV-pumping (fluorescence) and ignore contributions from direct (IR) excitation and collisions. The results from POPRATIO are shown by the curve in Fig. 19 as a function of the radiation field in Galactic units (G_0). Upper limits for N(Si II*) are derived from Si II$^\star\lambda$ 1264 which in turn yield upper limits on G/G_0, which is related to J

$$J = G \times 1 \times 10^{-19}\ \mathrm{erg\ cm^{-2}\ s^{-1}\ sr^{-1}\ Hz^{-1}}. \quad (10)$$

The luminosities in Table 9 are then combined with J in equation (6) to give a lower limit on the distance. These values are lower limits not just because of the non-detection of Si II*, but also because of our assumption that only UV-pumping contributes to the population of the fine-structure level. The lower limits derived are typically 15 to 30 kpc (see Table 9). Although these are considerably less stringent than the C II* distances, they are fairly robust and depend on very few assumptions and input parameters. The only caveat to this analysis is that at least two of the Si II transitions from the ground-state must be optically thin (Sarazin, Rybicki & Flannery 1979), which holds for all but one of our PDLA sample (which is excluded from this analysis).

In summary, we have used two methods to constrain QSO–PDLA distances. The C II* method (under the CNM assumption) gives a lower limit of 160 kpc for Q0151+048 (assuming no internal star formation), but is rather dependent on model assumptions. The Si II* model is more robust but gives less stringent limits, typically >15–30 kpc. Adding star formation to either method increases the inferred distance of the PDLA from the QSO. The distances imply that the absorbers are external to the QSO.

9 DISCUSSION

9.1 Sulphur and argon as indicators of QSO proximity

We have suggested that sub-solar ratios of [S/Si] at low values of N(H I) may be caused by the significant underestimate of N(S) from S II and, to a lesser extent, an overestimate of N(Si) from Si II in the presence of a hard ionizing spectrum. This result could be predicted from the photoionization models of Rix et al. (2007), who showed that the observed underestimate of sulphur is strongly dependent on the ionization parameter, U. Most models of intervening DLAs and sub-DLAs have concluded that the value of log U is typically < -3 (e.g. Howk & Sembach 1999; Dessauges-Zavadsky et al. 2003). However, for absorbers close to a QSO, the situation can be quite different. For example, Prochaska & Hennawi (2009) find that for a hydrogen volume density of 0.1 atoms cm^{-3} the ionization parameter of one of their transverse sub-DLAs at a distance of $\sim 100\,h_{70}^{-1}$ kpc from the QSO is log $U = -1.5$. The QSOs in our sample are typically a factor of 10 brighter than the case studied by Prochaska & Hennawi (2009), so ionization parameters in the range $-2 < \log U < 0$ are quite feasible.

Sub-solar [S/Si] ratios may therefore be used as a signpost of a nearby hard radiation source. Two of the intervening DLAs (FBQS 2334−0908 and PSS 0133+0400) in our literature sample also have [S/Si]< -0.5. One possible explanation could be that although they are intervening ($\Delta V \gg 10\,000$ km s^{-1}) systems, there is a nearby foreground QSO at a similar redshift. FBQS 2334−0908 is covered by the SDSS footprint. Although none of the objects near to FBQS

2334−0908 was targeted by the SDSS for spectroscopy, there are two point sources at separations of 27 and 105 arcsec (208 and 809 h_{70}^{-1} kpc at $z = 3$, respectively) whose colours are consistent with expectations of QSOs. PSS 0133+0400 is not covered by the SDSS, but the APM catalogue shows two point sources with similar colours to the QSO at separations of 57 and 64 arcsec (409 and 459 h_{70}^{-1} kpc at $z = 3.7$, respectively). It would be interesting to obtain spectra of these sources to determine whether or not they are indeed QSOs at the same redshift as the intervening DLAs. Indeed, some of the intervening N v absorbers identified by Fox et al. (2009) have nearby QSOs at the same redshifts (G. Worseck, private communication).

The low ratios of [Ar/Si] (where measured) in our PDLAs are also indicative of a hard ionizing spectrum (Vladilo et al. 2003). Using a sample of 10 Ar I measurements, Vladilo et al. (2003) have also found low ([Ar/Si] < -0.5) at $z_{\rm abs} < 3$. At higher redshifts, the values are close to, or at the solar level. Vladilo et al. (2003) have argued that this may be evidence for evolution in the ionizing background, which is shifting from a softer to harder shape as the redshift decreases. However, 3/7 of the $z_{\rm abs} < 3$ absorbers in the Vladilo et al. (2003) sample are PDLAs. A further two have velocities within 10 000 km s^{-1}, leaving only two which might be considered truly intervening absorbers. At $z_{\rm abs} > 3$ all three absorbers have $\Delta V > 15\,000$ km s^{-1}. Given the evidence presented in this paper that the effects of a hard ionizing spectrum are seen out to at least 3000 km s^{-1} (and previous results that indicate narrow associated absorbers may contribute out to 10 000 km s^{-1}; e.g. Wild et al. 2008; Tytler et al. 2009), the apparent redshift evolution may actually arise from the inclusion of proximate systems. A larger sample of large ΔV DLAs with argon measurements is necessary to more fully explore the redshift evolution of [Ar/Si].

9.2 N v as a tracer of high ionization gas

High ionization species such as N v and O VI might be expected to be more common in absorbers close to the QSO. Although O VI is blended in almost all of our sightlines, we have detections and upper limits of N v for all of our PDLAs. It is intriguing that the two detections of N v *at the same velocity as the singly ionized metal lines* are towards the two highest N(H I) absorbers (towards J1240+1455 and J1640+3951); both have log N(H I) > 21. However, both absorbers also have normal [S/Si] ratios, whereas we might expect departures from the solar ratio if the gas is partly ionized by a hard spectrum [as is seen for low N(H I) PDLAs]. The presence of N v in an ISM that is dominated by neutral gas indicates that the N v might be formed through an internal, localized source of ionizing radiation. In that case, the radiation from the QSO may not be responsible for the formation of the N v and the proximate nature of the DLA is misleading. Fox et al. (2009) found that the N v detection rate is higher for higher metallicity (intervening) DLAs. J1240+1455 and J1640+3951 have (undepleted) S abundances that are more than 1 dex higher than many of the other PDLAs in our sample and three times higher than intervening DLAs at the same N(H I) and redshift. Fox et al. (2009) have suggested that active star formation could be responsible for highly ionized gas which is consistent with the high metallicities, large velocity spreads and (for J1604+3951) the very high C II* column density. Indeed, Lehner et al. (2008) found that a pure QSO (hard) spectrum always underproduced the observed amount of N v in their study of a DLA with multi-phase gas; adding a soft stellar component significantly increased the predicted N v column density. Our own CLOUDY models indicate that even in the presence of a hard radiation field that is sufficient to produce sub-solar [S/Si] the N v/N I fraction is still only on the order of 10 per cent, which is consistent with the N v column density limits in our lower N(H I) systems.

Table 10. High ionization species offset from low ion detections. No offset high ions are detected for J0140−0839.

QSO	log N(H I)	$\Delta V_{\rm H\,I}$ (km s^{-1})	Velocity offset (km s^{-1})	High ions
J0142+0023	20.38 ± 0.05	1772	−100	C IV, Si IV
Q0151+048	20.34 ± 0.02	−1199	−825	N V, C IV
J1131+6044	20.50 ± 0.15	2424	−800	C IV,O VI
J1240+1455	21.3 ± 0.2	102	−125	N V
J1604+3951	21.75 ± 0.2	−656	−400	C IV, Si IV, N V
J2321+1421	20.70 ± 0.05	−1616	−100	C IV, Si IV

Both J1240+1455 and J1640+3951 show additional (and in the former case, much stronger) N v offset by several hundred km s^{-1} to the blue. A third PDLA (towards Q0151+048) shows highly offset N v (by −825 km s^{-1}) but no N v at zero velocity; in this case, the N(H I) is much lower, only log N(H I) = 20.34. It is notable that every PDLA in our sample of seven echelle spectra (with the exception of J0140−0839, which has very weak metal lines in general) has high ionization gas that is offset to negative velocities. In many cases, there is high ionization gas (such as C IV) at the redshift of the low ions but no low ions are seen to accompany the negative velocity high ion components. In some cases the velocity offset is small (e.g. C IV at ~ -100 km s^{-1} in J0142+0023). In other cases, the velocity offsets exceed −500 km s^{-1} (e.g. Q0151+048). We summarize these offset components in Table 10 (see Sections 4.2 to 4.7 for more detailed descriptions) listing both the ΔV of the PDLA from the background QSO and the velocity offset of the high ions from the main low ion components. Rix et al. (2007) also found a highly ionized component (observed in N v, C IV and Si IV) offset by $\sim +500$ km s^{-1} from the PDLA towards Q2343−BX415. Weidinger et al. (2005) find N v in two absorbers offset from a proximate Lyman limit system by a few thousand km s^{-1}. In these more extreme cases (e.g. Q0151+048), the absorption is likely to be unconnected with the proximate H I system and more akin to the associated high ionization associated systems studied by D'Odorico et al. (2004) and Fechner & Richter (2009).

For J1131+6044 and Q0151+048 where the high ion velocity offset is very high, it is likely that the absorption is arising in gas outside the PDLA. As discussed in Section 4.3, Q0151+048 has a fainter companion separated by 27.5 h_{70}^{-1} kpc and $\sim +120$ km s^{-1}. Although there is no confirmed companion for J1131+6044 in the NASA Extragalactic Data base (NED), the SDSS image shows a bright ($g = 17.59$) point-source 5.66 arcsec to the north-west. The object has an almost identical $g - r$ colour to J1131+6044 (0.41 and 0.38, respectively), so that this may be a binary QSO. The putative companion may contribute to the significant ionization seen in the J1131+6044 PDLA (e.g. high Si IV fraction), despite the large positive velocity offset from the QSO (2424 km s^{-1}; but see below for further discussion on the interpretation of velocities). The other five QSOs in our sample have no obvious bright companion within 20 arcsec on the SDSS image. If the companion to J1131+6044 is confirmed, this would mean that 2/7 of the QSOs with PDLAs in our sample have a close companion. Q2343−BX415 also has a companion, and its PDLA also has two distinct velocity components in the highly ionized gas, one of which is coincident with the bulk of the low ions, and the other offset by $\sim +500$ km s^{-1}.

9.3 The origin and nature of the PDLAs

The question that underpins the research of all associated absorbers is whether they are intrinsic to the QSO (host or outflow) or simply nearby in velocity space. Møller et al. (1998) examined a number of hypotheses for the nature of the PDLAs and favour a model in which the PDLAs are similar in nature to the intervening absorbers, but possibly located in a preferential environment, such as in the same overdensity as the QSO. Rix et al. (2007) suggest that the PDLA towards Q2343−BX415 (included in our literature sample) may be associated with outflowing material from the quasar host. Indirect clues to the provenance of the PDLAs may be garnered from their statistical properties. An excess of PDLAs relative to intervening systems has been confirmed by three studies (Ellison et al. 2002; Russell et al. 2006; Prochaska et al. 2008b). Although Ellison et al. (2002) found an additional excess of PDLAs in their radio-selected sample relative to optically selected QSOs, Russell et al. (2006) found an equal PDLA enhancement towards radio-loud and radio-quiet QSOs. The discrepancy may be due to the limited statistics of the Ellison et al. study, but a second possibility is the nature of radio sources. The CORALS sample used by Ellison et al. (2002) entirely comprises (rarer) flat-spectrum quasars that have compact morphologies. The sources detected at 20 cm in the Russell et al. (2006) sample will have a range of spectral indices and orientations. It would be interesting to investigate the dependence of PDLA incidence as a function of radio spectral index, as has been done extensively for C IV absorbers. There is certainly evidence that the quasar's radiation affects the ability of a PDLA to survive. Hennawi & Prochaska (2007) have shown that the incidence of transverse DLAs in projected QSO pairs overpredicts the incidence of proximate absorbers by a factor of 4–20. These authors suggested that line-of-sight PDLAs are preferentially photoevaporated by the QSO's beamed radiation. A similar overabundance of transverse Mg II absorbers relative to the line of sight has been seen by Bowen et al. (2006). Moreover, Prochaska et al. (2008b) show that despite the higher incidence of PDLAs relative to the intervening population, a clustering analysis indicates that they are none the less underabundant relative to the expected number density of galaxies near QSOs.

One of the observations that supports an intrinsic origin for many associated absorbers is their solar or super-solar metallicity (see the Introduction). We do not find any evidence for such elevated metallicities in our sample of PDLAs. The same is true of the associated Mg II systems (some of which may be DLAs) studied by vanden Berk et al. (2008). None the less, as discussed above, we do find that PDLAs with high H I column densities have a mean metallicity that is higher than intervening systems by around a factor of 3. For example, $[\mathrm{S/H}] = -0.88 \pm 0.24$ for the proximate absorbers versus -1.41 ± 0.20 for those at $\Delta V > 10\,000\,\mathrm{km\,s^{-1}}$. The correlation between stellar mass and gas-phase metallicity that exists out to redshifts of at least 3 (Tremonti et al. 2004; Savaglio et al. 2005; Erb et al. 2006; Maiolino et al. 2008) indicates that the PDLAs might therefore also be relatively massive. QSOs themselves are highly biased tracers of mass and are often located in or near galaxy clusters or other overdensities, although they apparently eschew the centres of clusters (Sanchez & Gonzalez-Serrano 1999; Barr et al. 2003; Sochting, Clowes & Campusano 2004; Kauffmann et al. 2004; Lietzen et al. 2009; Hutchings, Scholz & Bianchi 2009). Since the typical stellar mass of a galaxy tends to increase with the galaxy density of its local environment (e.g. Baldry et al. 2006), the combination of clustering and the mass–metallicity relation may explain the higher metallicities of PDLAs. Further evidence for this scenario comes from the discovery of a likely companion QSO to J1131+6044, and with the previously known companions of Q0151+048 and Q2343−BX415 (Møller et al. 1998; Rix et al. 2007). Boris et al. (2007) find evidence that 3/4 of the QSO binaries in their sample are associated with rich clusters at $z \sim 1$. Other evidence for absorbers clustered around QSOs comes from the incidence of transverse absorbers. In their study of close projected pairs (in which it is argued that transverse absorbers suffer less photoevaporation than line-of-sight absorbers) Hennawi et al. (2006) find a 50 per cent covering fraction of sub-DLAs within 150 kpc.

It may seem surprising that absorbers with velocity offsets of up to 3000 km s^{-1} could be considered associated with the QSO environment when this velocity corresponds to a Hubble flow distance of ~ 10 Mpc (proper) at $z \sim 3$. However, the velocity offsets are unlikely to indicate Hubble flow distances, as clearly demonstrated by the existence of absorbers with very negative velocities. Although we have additionally highlighted the uncertainty in the emission redshifts, these are unlikely to be incorrect by the >1500 km s^{-1} required to make all of our absorber offsets positive. We have discussed above some of the observations that have shown that QSOs often occupy overdense regions, a statement that might lead us to imagine cluster-like structures today with sizes of a few Mpc. However, Lietzen et al. (2009) have argued that QSOs can also trace out other overdense structures, such as filaments whose dimensions can be tens of Mpc. Haines, Campusano & Clowes (2004) have found evidence for an extreme structure of galaxies clustered around quasars on scales of tens of Mpc at $z \sim 1$.

The PDLAs appear to share some characteristics in common with absorbers associated with gamma-ray burst (GRB) hosts. The GRB DLAs have higher metallicities and are skewed to higher N(H I) than intervening QSO DLAs (e.g. Prochaska et al. 2007a). Higher [α/Fe] are also found in the GRB DLAs, similar to some of the PDLAs in our sample. However, the difference between the GRB DLAs and intervening systems is often attributed to the GRB sightlines preferentially intersecting the galaxy at smaller galactocentric radii, rather than a fundamental difference in the populations probed by the GRBs and QSOs.

Regardless of their origin, if the metallicities of [at least the high N(H I)] PDLAs are relatively high, as a population they present an interesting new selection technique for identifying the most metal-rich galaxies at high redshift. With metallicities ranging from 1/3 to 1/10 of the solar value, the high N(H I) PDLAs have metallicities similar to the 'metal-strong DLAs' (MSDLAs, Herbert-Fort et al. 2006) at $z \sim 2$ (Kaplan et al. 2010). Indeed, a number of MSDLAs are also PDLAs (Kaplan et al. 2010). Although this is still more metal-poor than the majority of Lyman Break Galaxies (LBG) studied at this redshift, most LBG abundances are limited to fairly massive galaxies (Erb et al. 2006). Gravitational lensing permits studies of fainter galaxies. Only a handful of such objects have been studied so far, but the results indicate that galaxies with $\sim L_\star$ luminosities at $z \sim 2$ to 3 have metallicities of $Z \sim 1/2\,\mathrm{Z}_\odot$ (e.g. Teplitz et al. 2000; Pettini et al. 2002; Quider et al. 2009, 2010). If the PDLAs follow a similar mass–metallicity relation, then they may be only slightly less massive than these lensed LBGs. High metallicity systems present a number of interesting possibilities for studying the high-redshift ISM. For example, Noterdaeme et al. (2008) have shown that molecular hydrogen is highly dependent on metallicity. High metallicities also present the opportunity to detect and study the abundances of rarely detected elements such as Ge, B, Cl and Co (Ellison, Ryan & Prochaska 2001a; Prochaska, Howk & Wolfe 2003c).

9.4 Future work

Hennawi et al. (2006) presented a sample of close, projected QSO pairs where the background quasar exhibits optically thick Lyα absorption at the redshift of the foreground quasar. It is shown that 50 per cent of projected QSO pairs have an absorber with $\log N(\mathrm{H\,I}) > 19$ at the redshift of the foreground QSO when the separation is < 150 kpc. This much higher incidence of transverse absorbers, relative to proximate line-of-sight absorbers, is suggested by Hennawi & Prochaska (2007) to be due to differential photoevaporation by anisotropic radiation of the foreground QSO. In the future, it will be interesting to compare the chemical abundances and ionization indicators of PDLAs to transverse DLAs at a given $N(\mathrm{H\,I})$ (e.g. Prochaska & Hennawi 2009) and to test fine-structure distance estimates against the measurable transverse separations.

Despite their external provenance, the QSO's radiation can apparently affect PDLAs out to at least 2500 km s^{-1} from the QSO. With a larger sample, and accurate redshifts, it will also be possible to look for trends with velocity. Ultimately, this may require the incorporation of other parameters such as QSO luminosity, including radiation from nearby companions. A campaign is currently underway to obtain IR spectra for a sample of QSOs with PDLAs (including those presented in this paper) that will yield redshifts accurate to $\sim$40 km s^{-1} from the [O III] λ 5007 line. It is worth noting that only a few tens of $z > 2$ QSOs have redshifts [O III] λ 5007 (e.g. Scott et al. 2000). For objects in the Hubble flow, velocities correspond to distances. For positive values of ΔV we cannot distinguish between these expansion velocities and peculiar motions (as expected if the galaxies and QSOs are in the same gravitational potential). However, negative ΔV cannot be due to Hubble expansion, since it would imply the absorber is more distant than the QSO, which is clearly impossible. The negative side of the velocity distribution of PDLAs therefore yields the 'true' velocity distribution of the PDLAs around the QSO, without contamination from the Hubble flow. Larger samples will also allow us to study trends of the combined effect of ΔV and QSO luminosity.

10 CONCLUSIONS

We have presented new high-resolution echelle spectra for seven PDLAs with $\Delta V < 3000$ km s^{-1}. The metal column densities derived from Voigt profile fits and the apparent optical depth method are complemented with abundances for a further nine PDLAs taken from the literature. Our PDLA sample is compared to the most complete sample of intervening DLAs currently available. Our principal conclusions are as follows.

(i) PDLAs exhibit a range of metallicities at a given redshift, ranging from $\sim$1/3 to 1/1000 of the solar value (Section 7.1 and Fig. 14). One of the PDLAs in our sample exhibits the lowest $N(\mathrm{Si\,II})/N(\mathrm{H\,I})$ of any known DLA and has a value similar to the intergalactic medium at this redshift.

(ii) Based on this modest-sized sample, there is a general trend (with the exception of one fairly high velocity PDLA) for low metallicities ($Z \sim 1/50\,\mathrm{Z}_{\odot}$) in PDLAs with $\log N(\mathrm{H\,I}) < 21$ and higher metallicities ($Z \sim 1/10\,\mathrm{Z}_{\odot}$) when the H I column density is higher (Fig. 15). At these high H I column densities, the metallicities of PDLAs are systematically higher than the intervening sample by a factor of around 3.

(iii) At least half of the PDLAs with $N(\mathrm{H\,I}) < 20.8$ have sub-solar ratios of [S/Si] which cannot be easily explained by known dust or nucleosynthetic trends (Section 6.3 and Fig. 13). We interpret the low values as resulting from ionization by a hard spectrum. Sub-solar values of [S/Si] can be present even in PDLAs with $\Delta V > 2000$ km s^{-1}, and with no obvious trend with velocity.

(iv) In addition to the dependence of metallicity on $N(\mathrm{H\,I})$ and the sub-solar [S/Si] ratios, other indications of enhanced/hard ionization in the PDLAs which distinguish them from the intervening DLAs are: (1) a possibly higher fraction of N V absorbers (tentative based on the small number statistics of our sample), (2) higher fractions of Si IV/Si II at low $N(\mathrm{H\,I})$, (3) similar velocity structure in Si IV as Si II in 3/5 QSOs where the comparison can be made, (4) low ratios of [Ar/Si] (Section 6).

(v) Most of the PDLAs (6/7) in our sample of seven have additional high ionization gas at large negative velocities of -100 to -825 km s^{-1} (Section 9.2 and Table 10). The most extreme examples both have either a confirmed (Q0151+048) or tentative (J1131+6044) close companion QSO.

(vi) One of the PDLAs in our sample has very sub-solar [Fe/Zn] consistent with a large dust depletion fraction. However, in general, the [Fe/Zn] ratios of the PDLAs are consistent with the intervening population (Section 7.2 and Fig. 16). The PDLA towards J1604+3951 has very different depletion in its two main components.

(vii) The range of α-to-iron ratios in the PDLAs are also consistent with the intervening DLAs, although there are a few notably high values (Section 7.3 and Fig. 17).

(viii) From analyses of the fine-structure lines of Si II and C II, QSO–absorber distances at least a few tens of kpc are determined, with one case being constrained to have a separation of >160 kpc (Section 8).

We conclude that PDLA properties are generally consistent with an origin external to the QSO host (in contrast with, e.g., the narrow line associated systems; D'Odorico et al. 2004). However, the larger abundances [at least of high $N(\mathrm{H\,I})$ PDLAs] imply that they may not be representative of the intervening sample. We suggest that the PDLAs may preferentially sample overdense environments where biased galaxy formation has assembled more massive galaxies with higher metallicities. Indeed, at low redshift, some associated absorbers have been identified with small clusters of galaxies (e.g. Bergeron & Boissé 1986; Hamann et al. 1997a). If confirmed with larger samples, this means that PDLAs could be used as probes of massive galaxies at high redshift.

PDLAs have been widely excluded from most DLA surveys. The results presented here indicate that, depending on the science objective, this is a valid approach. We have argued that PDLAs may sample a rather special population of DLAs, possibly those in proto-clusters. Although this renders the PDLAs an interesting probe of high-redshift galaxies, our results reveal some of the biases that could be introduced into statistical surveys that do not impose a ΔV limit in their DLA selection. A high priority for future work will be the improvement of emission redshift determinations. The results presented here imply that even at fairly large relative velocities ionization may affect abundance determinations. Determining more accurate ΔV-values in larger PDLA samples will provide an empirically motivated cut-off for studies of intervening DLAs.

ACKNOWLEDGMENTS

We are grateful to the following people for sharing data that enabled us to re-calculate emission redshifts for quasars in the literature: Andrew Fox, Johan Fynbo, Isobel Hook, Michael Murphy, Samantha Rix and Tayyaba Zafar. Nikola Milutinovic and Nicolas Tejos helped with the data acquisition of the HIRES and UVES

data, respectively. Andrew Fox, Palle Møller and Pasquier Noterdaeme provided useful comments on a draft of the paper. DMR acknowledges support from a Netherlands Organization for Scientific Research (NWO) Veni Fellowship.

REFERENCES

Aguirre A., Dow-Hygelund C., Schaye J., Theuns T., 2008, ApJ, 689, 851
Akerman C. J., Ellison S. L., Pettini M., Steidel C. C. 2005, A&A, 440, 499
Asplund M., Grevesse N., Sauval A. J., 2005, ASP Conf. Ser. 336, Cosmic Abundances as Records of Stellar Evolution and Nucleosynthesis in honour of David L. Lambert. Astron. Soc. Pac., San Francisco, p. 25
Asplund M., Grevesse N., Sauval A. J., Scott P., 2009, ARA&A, 47, 481
Baker J. C., Hunstead R. W., Athreya R. M., Barthel P. D., de Silva E., Lehnert M. D., Saunders R. D. E., 2002, ApJ, 568, 592
Bakes E. L. O., Tielens A. G. G. M., 1994, ApJ, 427, 822
Baldry I. K., Balogh M. L., Bower R. G., Glazebrook K., Nichol R. C., Bamford S. P., Budavari T., 2006, MNRAS, 373, 469
Barr J. M., Bremer M. N., Baker J. C., Lehnert M. D., 2003, MNRAS, 346, 229
Bergeron J., Boissé P., 1986, A&A, 168, 6
Boris N. V., Sodre L., Cypriano E. S., Santos W. A., de Oliveira C., West M., 2007, ApJ, 666, 747
Bowen D. V. et al., 2006, ApJ, 645, L105
Centurión M., Molaro P., Vladilo G., Péroux C., Levshakov S. A., D'Odorico V., 2003, A&A, 403, 55
Chen Y. Q., Nissen P. E., Zhao G., Asplund M., 2002, A&A, 390, 225
Cowie L. L., Songaila A., Kim T.-S., Hu E., 1995, AJ, 109, 1522
Dessauges-Zavadsky M., Péroux C., Kim T.-S., D'Odorico S., McMahon R. G., 2003, MNRAS, 345, 447
Dessauges-Zavadsky M., Calura F., Prochaska J. X., D'Odorico S., Matteucci F., 2007, A&A, 470, 431
D'Odorico V., Cristiani S., Romano D., Granato G. L., Danese L., 2004, MNRAS, 351, 976
Ellison S. L., Lewis G. F., Pettini M., Sargent W. L. W., Chaffee F. H., Foltz C. B., Irwin M. J., 1999, PASP, 111, 946
Ellison S. L., Songaila A., Schaye J., Pettini M., 2000, AJ, 120, 1175
Ellison S. L., Ryan S., Prochaska J. X., 2001a, MNRAS, 326, 628
Ellison S. L., Yan L., Hook I., Pettini M., Wall J., Shaver P., 2001b, A&A, 379, 393
Ellison S. L., Yan L., Hook I., Pettini M., Wall J., Shaver P., 2002, A&A, 383, 91
Erb D. K., Shapley A. E., Pettini M., Steidel C. C., Reddy N. A., Adelberger K. L., 2006, ApJ, 644, 813
Fechner C., Richter P., 2009, A&A, 496, 31
Fox A. J., Ledoux C., Petitjean P., Srianand R., 2007, A&A, 473, 791
Fox A. J., Bergeron J., Petitjean P., 2008, MNRAS, 388, 1557
Fox A. J., Prochaska J. X., Ledoux C., Petitjean P., Wolfe A. M., Srianand R., 2009, A&A, 503, 731
Fynbo J. U., Møller P., Warren S. J., 1999, MNRAS, 305, 849
Fynbo J. U., Burud I., Møller P., 2000, A&A, 358, 88
Ganguly R., Bond N. A., Charlton J. C., Eracleous M., Brandt W. N., Churchill C. W., 2001, ApJ, 549, 133
Gaskell C. M., 1982, ApJ, 263, 79
Haines C. P., Campusano L. E., Clowes R. G., 2004, A&A, 421, 157
Hamann F., Barlow T., Junkkarinen V., 1997a, ApJ, 478, 87
Hamann F., Beaver E. A., Cohen R. D., Junkkarinen V., Lyons R. W., Burbidge E. M., 1997b, ApJ, 488, 155
Hamann F., Barlow T. A., Junkkarinen V., Burbidge E. M., 1997c, ApJ, 478, 80
Hennawi J. F. et al., 2006, ApJ, 651, 61
Hennawi J. F., Prochaska J. X., 2007, ApJ, 655, 735
Hennawi J. F., Prochaska J. X., Kollmeier J., Zheng Z., 2009, ApJ, 693, L49
Herbert-Fort S., Prochaska J. X., Dessauges-Zavadsky M., Ellison S. L., Howk J. C., Wolfe A. M., Prochter G. E., 2006, PASP, 118, 1077
Holweger H., 2001, in Wimmer-Schweingruber R., ed., Solar and Galactic Composition. Springer, Berlin, p. 23
Howk J. C., Sembach K. R., 1999, ApJ, 523, L141
Howk J. C., Wolfe A. M., Prochaska J. X., 2005, ApJ, 622, L81
Hutchings J. B., Scholz P., Bianchi L., 2009, AJ, 137, 3533
Jorgenson R., Wolfe A. M., Prochaska J. X., Lu L., Howk J. C., Cooke J., Gawiser E., Gelino D., 2006, ApJ, 646, 730
Kaplan K. F., Prochaska J. X., Herbert-Fort S., Ellison S. L., Dessauges-Zavadsky M., 2010, PASP, in press
Kauffmann G., White S. D. M., Heckman T. M., Menard B., Brinchmann J., Charlot S., Tremonti C., Brinkmann J., 2004, MNRAS, 353, 713
Lehner N., Howk J. C., Prochaska J. X., Wolfe A. M., 2008, MNRAS, 390, 2
Leibundgut B., Robertson J. G., 1999, MNRAS, 303, 711
Lietzen H. et al., 2009, A&A, 501, 145
Lu L., Sargent W. L. W., Barlow T. A., Churchill C. W., Vogt S. S., 1996, ApJS, 107, 475
Lundgren B. F. et al., 2007, ApJ, 656, 73
Maiolino R. et al., 2008, A&A, 488, 463
Maza J., Wischnjewsky M., Antezana R., Gonzalez L. E., 1995, Rev. Mex. Astron. Astrof., 31, 119
Møller P., Jakobsen P., 1987, ApJ, 320, L75
Møller P., Warren S. J., 1993, A&A, 270, 43
Møller P., Warren S. J., Fynbo J. U., 1998, A&A, 330, 19
Nissen P. E., Chen Y. Q., Asplund M., Pettini M., 2004, A&A, 415, 993
Noterdaeme P., Ledoux C., Petitjean P., Srianand R., 2008, A&A, 481, 327
Noterdaeme P., Petitjean P., Ledoux C., Srianand R., 2009, A&A, 505, 1087
Petitjean P., Rauch M. J., Carswell R. F., 1994, A&A, 291, 29
Pettini M., Rix S., Steidel C., Adelberger K., Hunt M., Shapley A., 2002, ApJ, 569, 742
Pettini M., Zych B. J., Steidel C. C., Chaffee F. H., 2008, MNRAS, 385, 2011
Prochaska J. X., Hennawi J. F., 2009, ApJ, 690, 1558
Prochaska J. X., Wolfe A. M., 2002, ApJ, 566, 68
Prochaska J. X. et al., 2001, ApJS, 137, 21
Prochaska J. X., Gawiser E., Wolfe A. M., Castro S., Djorgovski S. G., 2003a, ApJ, 595, L9
Prochaska J. X., Gawiser E., Wolfe A. M., Cooke J., Gelino D., 2003b, ApJS, 147, 227
Prochaska J. X., Howk J. C., Wolfe A. M., 2003c, Nat, 423, 57
Prochaska J. X., Herbert-Fort S., Wolfe A. M., 2005, ApJ, 635, 123
Prochaska J. X., Chen H.-W., Bloom J. S., 2006, ApJ, 648, 95
Prochaska J. X., Chen H.-W., Dessauges-Zavadsky M., Bloom J. S., 2007a, ApJ, 666, 267
Prochaska J. X., Wolfe A. M., Howk J. C., Gawiser E., Burles S. M., Cooke J., 2007b, ApJS, 171, 29
Prochaska J. X., Chen H.-W., Wolfe A. M., Dessauges-Zavadsky M., Bloom J. S., 2008a, ApJ, 672, 59
Prochaska J. X., Hennawi J. F., Herbert-Fort S., 2008b, ApJ, 675, 1002
Prochaska J. X., O'Meara J. M., Worseck G., 2010, ApJ, submitted (arXiv:0912.0292)
Quider A. M., Pettini M., Shapley A. E., Steidel C. C., 2009, MNRAS, 398, 1263
Quider A. M., Shapley A. E., Pettini M., Steidel C. C., Stark D. P., 2010, MNRAS, 402, 1467
Richards G. T., 2001, ApJS, 133, 53
Richards G. T., York D. G., Yanny B., Kollgaard R. I., Laurent-Muehleisen S. A., vanden Berk D. E., 1999, ApJ, 513, 576
Richards G. T., Laurent-Muehleisen S. A., Becker R., York D. G., 2001, 547, 635
Richards G. T. et al., 2002, AJ, 124, 1
Rix S. A., Pettini M., Steidel C. C., Reddy N. A., Adelberger K. L., Erb D. K., Shapley A. E., 2007, ApJ, 670, 15
Russell D., Ellison S. L., Benn C. R., 2006, MNRAS, 367, 412
Sanchez S., Gonzalez-Serrano J., 1999, A&A, 352, 383
Sarazin C. L., Rybicki G. B., Flannery B. P., 1979, ApJ, 230, 456
Savage B. D., Sembach K. R., 1991, ApJ, 379, 245
Savaglio S. et al., 2005, ApJ, 635, 260
Schaye J., Carswell R. F., Kim T.-S., 2007, MNRAS, 379, 1169
Scott J., Bechtold J., Dobrzycki A., Kulkarni V. P., 2000, ApJS, 130, 67

Shen Y. et al., 2007, AJ, 133, 2222
Silva A. I., Viegas S. M., 2002, MNRAS, 329, 135
Simcoe R. A., Sargent W. L. W., Rauch M., 2004, ApJ, 606, 92
Sochting I. K., Clowes R. G., Campusano L. E., 2004, MNRAS, 347, 1241
Sofia U. J., Jenkins E. B., 1998, ApJ, 499, 951
Songaila A., 1997, ApJ, 490, L1
Srianand R., Petitjean P., 2000, A&A, 357, 414
Srianand R., Petitjean P., Ledoux C., Ferland G., Shaw G., 2005, MNRAS, 362, 549
Teplitz H. I. et al., 2000, ApJ, 533, L65
Tremonti C. et al., 2004, ApJ, 693, 898
Tytler D., 1982, Nat, 298, 427
Tytler D., Fan X.-M., 1992, ApJS, 79, 1
Tytler D. et al., 2009, MNRAS, 392, 1539
vanden Berk D. E. et al., 2001, ApJ, 122, 549
vanden Berk D. E. et al., 2008, ApJ, 679, 239
Vestergaard M., 2003, ApJ, 599, 116
Vladilo G., Centurion M., Bonifacio P., Howk J. C., 2001, ApJ, 557, 1007
Vladilo G., Centurion M., D'Odorico V., Peroux C., 2003, A&A, 402, 487
Vogt S. S., 1994, in Ulrich M.-H., ed., ESO Conf. and Workshop Proc. 40, High Resolution Spectroscopy with the VLT. ESO, Garching, p. 223
Vreeswijk P. et al., 2007, A&A, 468, 83
Weidinger M., Møller P., Fynbo J. P. U., Thomsen B., 2005, A&A, 436, 825
Wild V. et al., 2008, MNRAS, 388, 227
Wise J. H., Eracleous M., Charlton J. C., Ganguly R., 2004, ApJ, 613, 129
Wolfe A. M., Prochaska J. X., 2000, ApJ, 545, 591
Wolfe A. M., Lanzetta K. M., Foltz C. B., Chaffee F. H., 1995, ApJ, 454, 698
Wolfe A. M., Prochaska J. X., Gawiser E., 2003, ApJ, 593, 215
Wolfe A. M., Prochaska J. X., Jorgenson R. A., Rafelski M., 2008, ApJ, 681, 881

This paper has been typeset from a TEX/LATEX file prepared by the author.